Registration number,
"Petru Poni" Institute
of Macromolecular Chemistry

_____3324/30.06.2022_____

SCIENTIFIC STAGE REPORT

PN-III-P4-ID-PCCF-2016-0050 Project. Contract no. 4/2018.

-- 2022 Stage --

Mimicking Living Matter Mechanisms by Five-dimensional Chemistry Approaches

Mimarea mecanismelor viului prin abordări ale chimiei supramoleculare, în cinci dimensiuni

Acronym: 5D-nanoP

Project WEB site: https://www.intelcentru.ro/5D-nanoP/ro/ and https://www.intelcentru.ro/5D-nanoP/

Objective of 2022 stage: ***Elaboration of a know-how blueprint on the design, production and testing of supramolecular nanoplatforms***

Synopsis of the stage results:

As a final phase of the project, the 2022 stage was dedicated to the refinement of the experimental approaches and to the drafting of a know-how blueprint on the practical solutions previously developed. Particular attention was paid to the nanoplatforms construction and to the development of surrogate biological milieus for nanoentities testing.

In terms of scientific production, the 2022 stage was materialized in 28 papers published in ISI ranked journals, 1 book chapter, 12 oral/poster communications, 2 keynote conferences, two meetings between partners (online), a final workshop (online), and 1 research stay.

Project Director,
Prof. Aatto Laaksonen

*This report summarizes work performed on the **5D-nanoP** project during the period January - June 2022.*

Stage 2022 Work Plan

Code	Activities carried out during the 2022 stage of 5D-nanoP project (January – June 2022)
5.1.	**Finalization of protocols for synthesis and characterization of nanoplatform constituents**
5.1.1.	- *In silico* studies on dynamic remodeling of nanoentities supramolecular morphology.
5.1.2.	- Targeting carbonic anhydrases as natural nanoentities.
5.1.3.	- Systems based on silatrane and glucose-functionalized mesoporous silica.
5.1.4.	- Silica-containing functional ligands.
5.1.5.	- Electroactive macromonomers as building blocks for electro-chemo-bioactive conjugated graft copolymers.
5.1.6.	- Preparation, and characterization of lipopolyplexes (LPP) functionalized with a peptide recognizing VCAM-1 and encapsulating C60-PEI/shRunx2 polyplexes (V-LPP/shRunx2) and validation on their functionality in reducing the osteogenic differentiation of aortic valve interstitial cells.
5.2.	**Finalizing the procedures for obtaining and characterizing nanoplatforms**
5.2.1.	- Structural characterization and properties investigations of the nanoplatforms constituents.
5.2.2.	- Strategies for nanoplatforms construction based on grafted conjugated electro-conducting polymers (g-CPs).
5.3.	**Finalization of protocols and procedures for obtaining and characterizing matrices for *ex vivo* testing of nanoplatforms**
5.3.1.	- Hyaluronic acid - poly(methylvinylether-*alt*-maleic acid) hydrogels as surrogates for bio-medical testing.
5.3.2.	- Alginate-poloxamer hydrogels produced by photo-initiated thiol-ene reaction.
5.3.3.	- Curdlan and curdlan derivatives as surrogates for biomedical applications.
5.3.4.	- Protocols for testing the matrices' cytocompatibility and their use as tumor/tissue surrogates.
5.4.	**Finalization of protocols for testing the functionality of nanoplatforms**
5.4.1.	- Protocols for testing nanocarriers for controlled delivery of antitumor drugs to cancer cells.
5.4.2.	- Characterization techniques used for the bio-electroactive nanoplatforms.
5.5.	**Elaboration of documentation on obtaining and characterizing nanoplatforms. Estimation of potential applications.**

The research results of 2022 stage
The report can be found at https://www.intelcentru.ro/5D-nanoP/

5.1. Finalization of protocols for synthesis and characterization of nanoplatform constituents

5.1.1. *In silico* studies on the dynamic remodeling of nanoentities supramolecular morphology

In silico studies in 5DnanoP serve several purposes, from giving guidance to synthesis (and post-synthesis) and assisting in characterization performed in virtually all non-label experimental techniques found in the instrumental park of IntelCentru laboratory and "Petru Poni" institute. *In silico* provide means for screening large data sets to narrow leads of components of drug delivery systems and vehicles. *In silico* groups works in a wide range, from model development to large-scale high-performance computing, of 5DnanoP related biomolecular systems. The novel aspect in the activity of the *in silico* group is working very intimately with the laboratory partners, by using similar protocols as in the corresponding experiments. This in turn requires for the simulations extensive system (sample) sizes and very long time-scales to be covered. We use regularly supercomputers in the most demanding computations.

PTh-*g*-(PEG-*ran*-PCL) amphiphilic heterografted polymer as part of nanoplatforms and of drug/gene delivery system has been on focus in 2022 too. This is originally PhD work of Petru Tîrnovan. Tudor Vasiliu and Răzvan Puf also worked in a nice collaboration with 5DnanoP partners where the synthesis and characterization are performed by the group of Dr. Cianga, while we have built a replica of the same system suitable for simulations studies of how it can be conformationally modulated using different solvent media, for example, to collapse over drug/gene material (***Figure 1***). We are currently writing two articles on this subject.

Propiconazole nitrate and its cyclodextrin inclusion complexes and the role of cosolvents were studied by Dragoș Isac and Andrei Neamțu. As the complexes are poorly soluble in water mixed solvent

water: DMSO was applied, showing excellent solvent properties. ***Figure 2*** shows both radial and spatial distribution functions of the equimolar mixture of H_2O : DMSO efficiently solvating the inclusion compound.

The new type of **non-viral vectors made of polypeptide HIS3 with a starlike core** were created and modeled by Tudor Vasiliu and Dragoş Peptanariu, and it complexation with DNA was studied in extended MD simulations (***Figure 3***). Based on the properties of HIS3 polypeptide, the star-like vector also acts as a nanoplatform for synthesis or for organizing supramolecular interactions.

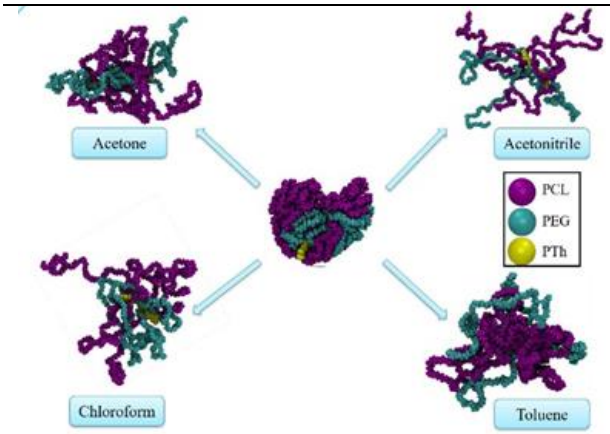

Figure 1. *Supramolecular conformation control of PTh-g-(PEG-ran-PCL) amphiphilic heterografted polymers by means of organic solvent, as a basis of branches exposure for further reactions or supramolecular inetractions.*

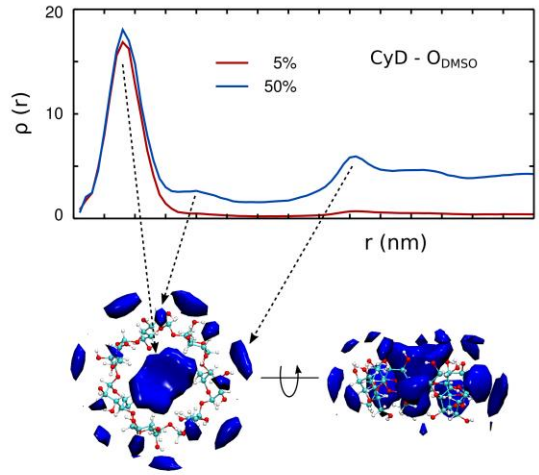

Figure 2. *In silico model of propiconazole - cyclodextrin inclusion complex solvated in water : DMSO mixtures.*

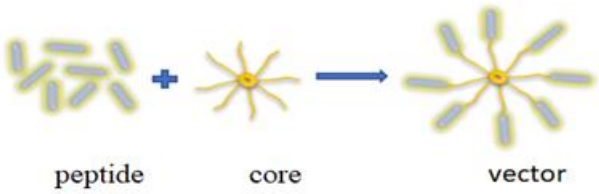

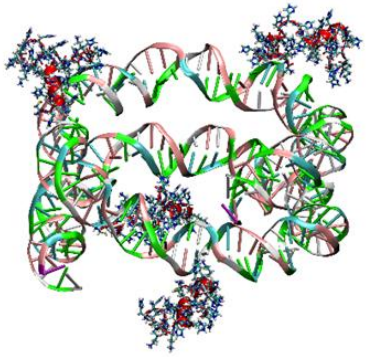

Principle of vector producing. *Vector interaction with DNA.*

Figure 3. *The structure and use of star-like vectors containing terminal polypeptides.*

5.1.2. Targeting carbonic anhydrases as natural nanoentities

The investigation of the particular functionality of Carbonic Anhydrase (CA, EC 4.2.1.1) family as natural nanoentities was continued, in terms of the modulation of their enzyme activity by involving potential inhibitory unimers. The dynamically generated supramolecular assemblies were studied for

three of the most active inhibitors: (**i**) monosulfamyl compounds of pharmaceutical relevance, (**ii**) organotelluride compounds, and (**iii**) pyrazolo[4,3-c]pyridine sulfonamides.

I. Kinetic and crystallographic studies of azosemides as a selective inhibitor of CA isoforms, by the tail approach.

The main scope of the drug design campaigns in the last years has been to obtain isoform-selective CAIs for the 13 humans catalytically active CAs isoforms specifically involved in different pathologies. In this context, by kinetic and crystallographic studies, we investigated the sulfonamide loop diuretic Azosemide (***Figure 4A***) developed by Boehringer Mannheim GmbH and brought to market in 1981, in comparison with the analog furosemide, in order to understand the key points for isoform selective compounds by the tail approach.

A

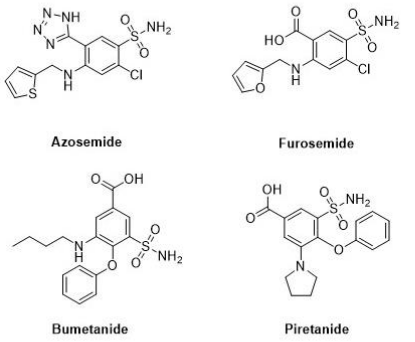

B

K_i (nM)*				
Cmp	**Azosemide**	**Furosemide[a]**	**bumetamide[a]**	**AAZ**
hCA I	51.8	62	4930	250
hCA II	64.4	65	6980	12.1
hCA III	>10000	$3.2\ 10^6$	$3.4\ 10^6$	$2\ 10^5$
hCA IV	13.9	564	303	74
hCA Va	243.2	499	700	63
hCA Vb	93.3	322	159	54
hCA VI	93.8	245	3890	11
hCA VII	8.9	513	62	2.5
hCA IX	137.5	420	25.8	25.8
hCA XII	89.2	261	21.1	5.7
hCA XIII	201.9	550	2570	17
hCA XIV	8.8	52	250	41

C

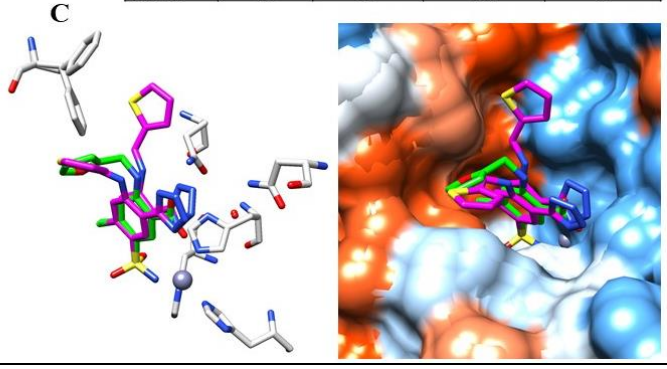

Figure 4. *(**A**) Structures of loop diuretics; (**B**) Inhibition data of human CA isoforms; (**C**) Overlay of azosemide (magenta) and furosemide (green, PDB: 1Z9Y) with hCA II; Hydrophobic (red) and hydrophilic (blue) residues in the inhibitory site of CAs are labeled.*

The inhibition profile (***Figure 4B***) shows the same high potency as the structural analog loop diuretic furosemide towards the most abundant isoforms hCA I and hCA II. However, the simple replacement of the carboxylic group with a bulkier tetrazole moiety, leads to important differences in the inhibition profile for the other isoforms present in the kidney, such as hCA XII, and in particular against hCA IV and XIV, thus explaining possible differences of potency *in vivo*. The higher inhibitory potency of azosemide compared to furosemide and bumetanide against hCA VII might also explain its efficacy in the management of epilepsy. In addition, the structural superimposition between azosemide and furosemide in a complex with hCA II (***Figure 4C***) did not show significant differences in the location of the inhibitor inside the active site, except the tails where the furanylmethylamino tail of furosemide is located in the same hydrophobic region occupied by one of the two conformations observed for the thiophene ring of azosemide (***Figure 4C***).

II. Carbonic anhydrase inhibitors bearing organotelluride moieties as novel redox imbalance agents for antitumor therapy.

Continuing our studies on the antitumor effects of several CA inhibitors, we synthesized a novel series of organotellurides bearing sulfonamide moiety as innovative CAIs (***Figure 5A***). The high and selective CA inhibition against the tumor-associated isoforms hCA IX and XII, as well as the cytosolic hCA VII involved as ROS scavenger can be employed as a delivery platform to target the tumor cells without damaging the healthy tissue by ROS production, by our organotellurides.

The redox proprieties of our compounds were investigated by Electron Spin Resonance (ESR) experiments, as inhibitors of superoxide anion radical ($O_2^{\bullet -}$), hydroxyl radical ($HO^{\bullet}$) and as lipid peroxidation inhibitory (***Figure 5B***, ***5C***). The data in our hands showed these compounds, under certain

conditions, acting as oxidants or with different conditions acting as antioxidant agents. The oxidant property is sustained by indirect evidence, obtained from cell line experiments (***Figure 5D***), where an increase in oxidative stress was observed following their treatment with our compounds, and by ESR experiments. Overall, the organotellurides **5-7** showed unique and interesting redox features and they can be used as innovative therapeutic approach against different hypoxic tumors.

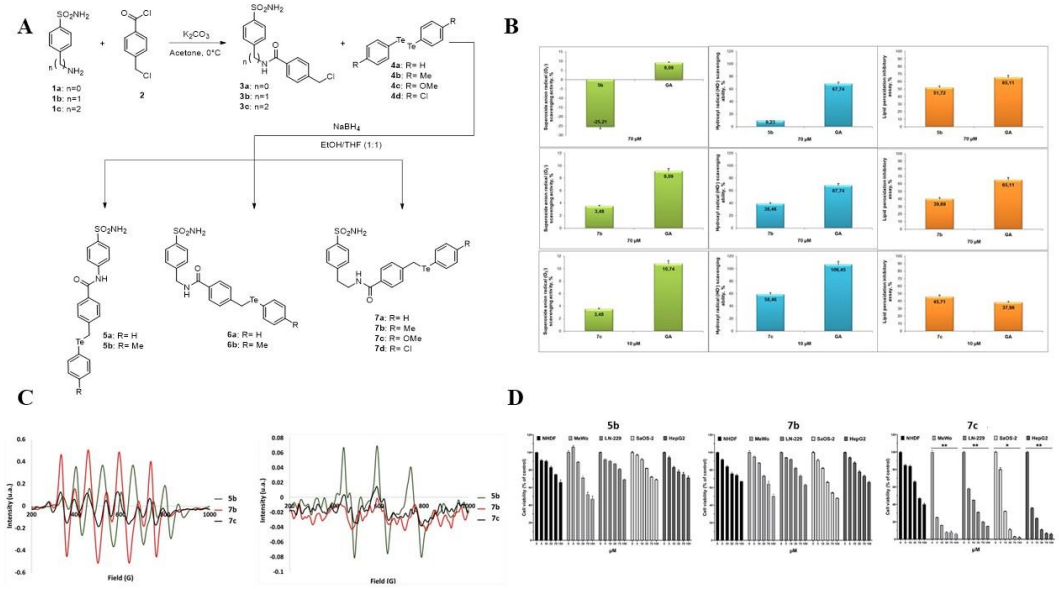

Figure 5. *(**A**) The synthesis of carbonic anhydrase inhibitors bearing organotelluride moieties. (**B**) Superoxide anion radical ($O_2^{\bullet -}$), hydroxyl radical ($HO^{\bullet}$) scavenging ability and Lipid peroxidation inhibitory capacity of studied compounds. (**C**) ESR spectra of the radicals generated by the compounds 5b, 7b and 7c in DMSO in the presence of DMPO or PBN. (**D**) Cytotoxicity of 5b, 7b and 7c (0, 5, 10, 30, 70 and 100 μM) on normal human dermal fibroblasts (NHDF), malignant melanoma (MeWo), glioblastoma (LN-229), osteosarcoma (SaOS-2) and hepatocellular carcinoma (HepG2) cells.*

III. Pyrazolo[4,3-c]pyridine sulfonamides as carbonic anhydrase inhibitors: synthesis, biological and in silico studies.

Pyrazole and pyrazolopyridine scaffolds are adaptable molecules that are present as structural motifs in several drug molecules. Two different groups of compounds were evaluated for their inhibitory activities towards four human CAs (I, II, IX, and XII) as well as 3 β- and 3- γ CAs from different bacterial strains such as *E. coli*, *Burkholderia pseudomallei*, *Vibrio cholerae*. Five out of eleven compounds were more potent than reference drug acetazolamide (AAZ) against the hCA II isoform. As far as the inhibition of the β- and γ-CAs from different bacterial strains showed good activity. Furthermore, computational procedures were used to investigate the binding mode of this class of compounds (***Figure 6***).

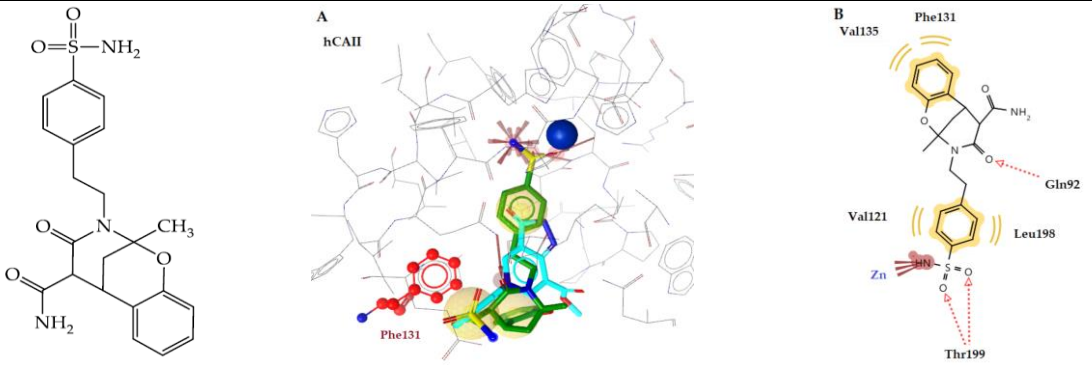

Figure 6. *One of the investigated pyrazolo[4,3-c]pyridine sulfonamides. (**A**) Accommodation inside of hCA II inhibitory site. (**B**) 2D interaction diagram with the key amino acids in hCA II. Active-site zinc shown as blue sphere, red dotted arrows indicate H-bond, and yellow spheres are hydrophobic interactions.*

5.1.3. Systems based on silatrane and glucose-functionalized mesoporous silica

In this stage the protocols for the synthesis and characterization of the nanoplatform constituents were validated on the following studied class of compounds (***Figure 7***):

- 3-aminopropylsilatrane and its Schiff base derivative: 1-(3-{[(2-hydroxy-5-nitrophenyl)-methylidene]amino}propyl)silatrane; the spectroscopic characterization proce-dures (FT-IR, NMR, UV-vis, fluorescence) confirmed the structure, the functionalities and the stability assessment of biodegradable and bioactive segments;
- the thiol- and glucose-functionalized mesoporous silica; the spectroscopic characterization procedures (FT-IR, Raman, UV-vis, fluorescence) confirmed the structure, and cytotoxicity tests assessed the biocompatibility of the biodegradable and bioactive segments.

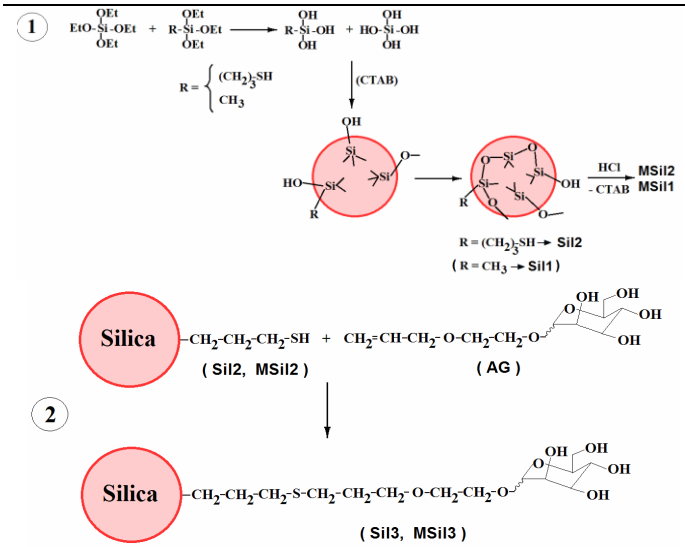

Figure 7. *The synthesis of thiol- and glucose-functionalized silica derivatized nanoplatforms.*

5.1.4. Silica-containing functional ligands

A. *Silatranes*:

A.1. Obtaining procedure (reactions in ***Figure 8***): A solution of 3-aminopropyl silatrane, SIL M, (0.100 g, 0.43 mmol) in chloroform (5 mL) is added to a solution of 2-hydroxy-5-nitrobenzaldehyde (0.072 g, 0.43 mmol) in acetonitrile (5 mL). The color turns orange-yellow. The mixture is stirred at room temperature overnight, then filtered, and allowed to crystallize at room temperature. Crystals formed by slow evaporation of the solvents are filtered, washed with a mixture of acetonitrile/chloroform solvents, and dried at room temperature.

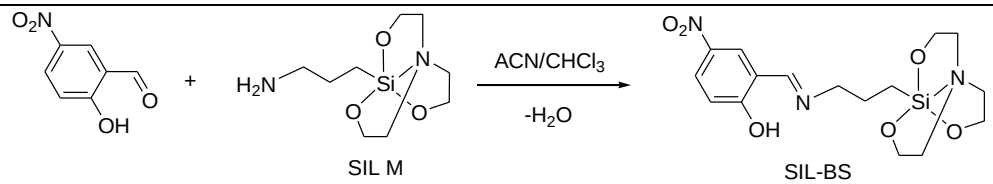

Figure 8. *Synthesis of silatrane-derivatives bearing nitro groups.*

A.2. Purification: Recrystallisation from acetonitrile, 48% (0.078 g)

A.3. Characterization procedure: spectroscopic methods (UV-vis, fluorescence, circular dichroism), biocompatibility/cytotoxicity, and molecular docking assessments. Thus, the ability of the constituents to bind proteins from bovine and human serum, the ability to inhibit the growth of normal (NHDF) and tumor cells (HepG2 and MCF7) or the inhibitory effect on viruses (SARS CoV-2), fungi, and bacteria was estimated.

B. *Dox-loaded silica materials*:

B.1. Obtaining procedure: Mesoporous silica MSil1 and MSil2 were obtained by co-hydrolysis of alkoxysilanes using CTAB surfactant as a template, in an alkaline medium, followed by template elimination in acidic conditions. Mesoporous silica with glucose groups (MSil3) was obtained by thiol-ene photoaddition: to a solution of allyloxyethylene-glucopyranoside (AG) (260 mg in 16 mL distilled

water), 84 mg of MSil2 and 9 mg of 2,2-dimethoxy-2-phenylacetophenone (DMPA) were added and the mixture was UV-irradiated at 365 nm for three periods of 10 minutes each, intercalated with 1 minute sonication with a UTR200 ultrasonic processor at 0.4 cycle and 40% amplitude.

B.2. Purification: The silica is centrifuged at 6000 rot/min for 10 minutes, separated, washed with water with centrifugation three times, separated and dried in a vacuum.

B.3. Characterization procedure: spectroscopic methods (FT-IR, Raman, UV-vis, fluorescence), biocompatibility/cytotoxicity and molecular dynamics assessments. Thus, the ability of the constituents to bind doxorubicin and the ability of the nanoplatforms to inhibit the growth of normal (NHDF) and tumor cells (HeLa, Mewo) were estimated.

C. *1-(3-{[(2-hydroxy-5-nitrophenyl)methylidene]amino}propyl) silatrane*

C.1. Obtaining procedure: amino-carbonyl condensation (iminization) in solution (chloroform / acetonitrile 1/1) at room temperature.

C.2. Characteristics:

- *Structural footprint*:

IR ν_{max} (KBr), cm^{-1}: 3466m, 3380m, 3356m, 3152w, 2924m, 2882m, 1658s, 1610vs, 1541s, 1483m, 1445m, 1406w, 1325vs, 1290s, 1274s, 1232s, 1188m, 1176m, 1163m, 1120s, 1090vs, 1051s, 1020s, 1006m, 938m, 910s, 833m, 798m, 779s, 756s, 715s, 685m, 627m, 578m, 547w, 526w, 505w, 482w, 403vw.

^{1}H NMR (DMSO-*d6*, 400.13 MHz) δ (ppm): 14.07 (s, 1H, OH, **H16**), 8.71 (s, 1H, -CH=N-, **H10**), 8.42 (d, J=3 Hz 1H, Ar-H, **H12**), 8.01 (dd, J=3 Hz, 1 H, Ar-H, **H15**), 6.54 (d, J=10 Hz, 1H, Ar-H, **H14**), 3.62 (t, J=6 Hz, 6H, **H1**, **H3**, **H5**), 3.57(t, J=7 Hz ,2H, **H9**), 2.80 (t, J=6 Hz, 6H, **H2**, **H4**, **H6**), 1.69 (s, J= 5 Hz, 2H, **H8**), 0.20 (q, J=3 Hz, 2H, **H7**).

^{13}C NMR (DMSO-*d6*, 100.13 MHz) δ (ppm): 179.02 (**C16**), 166.89(-CH=N-, **C10**), 133.06 (**C12**), 132.94 (**C13**), 129.30 (**C15**), 123.21 (**C14**), 112.95 (**C11**), 56.59 (**C1**, **C3**, **C5**), 54.41 (**C9**), 49.88 (**C2**, **C4**, **C6**), 25.93 (**C8**).

- *Molecular structure obtained by Single Crystal X-Ray Diffraction analysis* (see Figure 9).

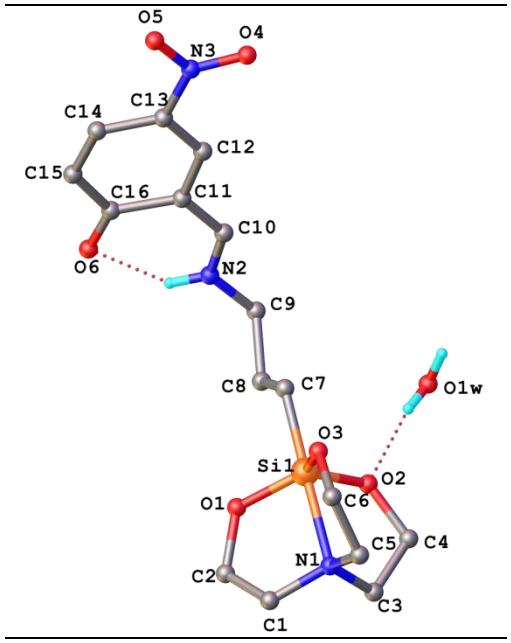

Figure 9. *Single Crystal X-Ray diffraction structure of 1-(3-{[(2-hydroxy-5-nitrophenyl)methylidene]-amino}propyl) silatrane.*

- *Registration number in Cambridge Crystallographic Data Centre*: CCDC 2175508

- *Stability in solution*: Absorption spectra (UV-vis): UV-vis (λmax (ε, $M^{-1}cm^{-1}$)): PBS (pH 7.4): 364 (25342), 388 (28540); PBS (pH 5): 320 (17864), 394 (1132); PBS (pH 1.5): 312 (20320), 396 (1321); DMSO: 368 (27500), 410 (33796); acetonitrile: 358 (18450), 404 (20708); dichloromethane: 356 (28594), 408 (28784); methanol: 352 (16300), 392 (16426); THF: 354 (20436), 406 (21148).

- *Cytotoxicity*: MCF7- IC_{50} 65 μg/mL; HepG2 - IC_{50} 150 μg/mL.

- *Protein binding* (Protein-Ligand nanoplatform): BSA K_b = $4.43 \cdot 10^5$ M^{-1} estimated by fluorescence studies. HSA K_b = 0.148 μM estimated by molecular docking.

- *Antimicrobial activity*: moderate on fungi species (*Aspergillus fumigatus*, *Penicillium frequen-tans*, *Fusarium sp.*) approximately three times smaller than Caspofungin; moderate on bacteria species (*Bacillus sp.*, *Pseudomonas sp.*) approximately twice as small as Kanamycin; -antiviral- comparable with chloroquine, E_b= -5.794 kcal/mol.

- *Mucoadhesiviness* on porcine small intestine mucosa: F = 0.092 N, W_a = 0.013 N · s.

D. *Three mesoporous slilica products*: (**4.1**) methyl-mesoporous silica (MSil1), (**4.2**) 3-mercapto-propyl-mesoporous silica (MSil2), (**4.3**) glucoside-propylene-oxy-ethylene-thiopropyl-mesoporous silica (MSil3).

D.1. Obtaining procedure: co-hydrolysis of alkoxysilanes assisted by CTAB surfactant as templating agent, in alkaline medium leading to silica, followed by elimination and silica derivatization through thiol-ene photoaddition.

D.2. Characteristics:

- *Structural footprint*:

MSil1: IR ν_{max} (KBr), cm^{-1}: 3451w, 2972vw, 2928vw, 2856vw, 1634vw, 1414vw, 1279m, 1069vs, 941vw, 800m, 567vw, 453m. **MSil2**: IR ν_{max} (KBr), cm^{-1}: 3443w, 2928w, 2856w, 1635w, 1074vs, 953m, 802w, 569w, 457s. **MSil2**: Raman (633 nm), cm^{-1}: 2924vs, 2900vs, 2856s, 2578w. 1442s, 1413m, 1308m, 1251m, 1038m, 813m,

759m, 507m. **MSil3**: IR ν_{max} (KBr), cm^{-1}: 3443m, 2928w, 2856w, 1727sh, 1687sh, 1636w, 1485vw, 1462vw, 1074vs, 955m, 802w, 698vw, 571w, 459s. **MSil3**: Raman (785 nm), cm^{-1}: 2909vw, 2855vw, 1683m, 1608m, 1597m, 1449m, 1417m, 1310m, 1213m, 1041m, 1023m, 1000s, 691s, 630s, 614s.

- *Cytotoxicity*. Cell viability at 50 μg/mL (%): MSil1/NHDF 82, MSil1/MeWo 84, MSil1/HeLa 72; MSil2/NHDF 86, MSil2/MeWo 91, MSil2/HeLa 76; MSil3/NHDF 88, MSil3/MeWo 87, MSil3/HeLa 78.

- *Doxorubicin binding* (Drug-Ligand nanoplatform): Dox: AG $K_b = 9.75 \cdot 10^4\ M^{-1}$; Dox: R-SH $K_b = 5.72 \cdot 10^4\ M^{-1}$ (estimated by fluorescence studies on model compounds).

- *Cytotoxicity of Dox-loaded silica*. Cell viability at 50 μg/mL (%): MSil1D/NHDF 29, MSil1D/MeWo 6, MSil1D/HeLa 6.6; MSil2D/NHDF 26, MSil2D/MeWo 11, MSil2D/HeLa 1.6; MSil3D/NHDF 47, MSil3D/MeWo 24, MSil3D/HeLa 18.

5.1.5. Electroactive macromonomers as building blocks for electro-chemo-bioactive conjugated graft copolymers (g-CPs)

End-group functionalization of homopolymers with a polymerizable moiety is certainly one of the most important milestones of polymer chemistry. It paved the way toward macromolecular architectural complexity, allowing the change from linear to nonlinear architecture through the so-called "macromonomer" or "grafting-through" strategy. This powerful approach has based on the strategy for the synthesis of the nanoplatforms constituents in the frame of 5DnanoP project. More precisely on the synthesis of electroactive macromonomers. They are important building blocks, the use of which has enabled the enlargement of the CPs “hairy-rods” class and has allowed for well-defined oligomeric/polymeric flexible side chains to be attached to the conjugated, rigid backbones, resulting in graft **rod-coil** type polymers with self-assembling propensity and high flexibility in the tuning of properties. Thus, the side chains can induce new properties to g-CPs, such as water-dispersibility and “stealth behavior”, thermo- and pH-sensitivity, intrinsic stretchability and self-healing properties or biocompatibility and partial biodegradability. These functionalizations facilitated the entrance of CPs into the field of biomaterials, synergistically fitting the goal of imparting electronic conductivity to biomaterials.

Electroactive macromonomers, so named due to their ability to polymerize oxidatively using electrochemical techniques, are also active in chemically oxidative polycondensation or, alternatively, in other polymerization methods specifically designed to obtain conjugated polymers (CPs). Basically, the controlled polymerization techniques were adopted and three different methods were applied for the synthesis of the electroactive macromonomers: (i) α-functionalization or the so-called “initiation method” (Th-PCL; EDOT-PCL), which made use of a functionalized initiator in a controlled ring-opening type polymerization (ROP) of e-caprolactone, (ii) ω-functionalization, which was accomplished by PEG post-polymerization functionalization (Th-PEG, DBrTh-PEG) modifying the existing chain ends with the thiophene desired functionality; (iii) the combination of (i) and (ii) variant for Th-OMeOx synthesis by using cationic ring-opening polymerization (CROP) with a thiophene-containing initiator for α-functionalization and ending of the reaction with an alcoholic solution of KOH for placing of –OH functionality at the ω-end of the oligo-(2-methyl-2-oxazoline) (OMeOx) chain.

The design criteria taken into account for their structures are presented in ***Figure 10.A***. Thus, the flexible polymers able to coil-up in solution were biocompatible and/or biodegradable polymers (PEG, PCL, OMeOx), of crystalline or amorphous nature in the solid state, two of them with water solubility. All of these polymers are able to accommodate ions, which is an advantage when interacting with the biological media is considered. For the aromatic part, our option focused on the thiophene or EDOT as thiophene-derivative based on the knowledge that polythiophenes are useful biomaterials. The most important property is their polymerizability, besides which the self-assembling ability by π-π interactions and the photosensitivity are important aspects as well. The presence of the hydroxyl ω-end groups for PCL and OMeOx endows the derived electroactive macromonomers with hydrogen-bonding ability in solution and in the solid state.

5.1.6. Preparation and characterization of lipopolyplexes (LPP) functionalized with a peptide recognizing VCAM-1 and encapsulating C60-PEI/shRunx2 polyplexes (V-LPP/shRunx2), and validation of their functionality in reducing the osteogenic differentiation of aortic valve interstitial cells.

The C60-PEI/shRNA polyplexes were obtained by mixing the C60-PEI and shRNA plasmids at a N/P ratio of 25. Cysteine-bearing VCAM-1 binding peptide (NH_2-VHPKQHRGGSKGC-COOH) or scrambled peptide (NH2-HVKHRQPGGSKGC-COOH) were coupled to polyplexes (***Figure 11***). First,

the peptides were incubated with a reducing agent (TCEP) for 2 hours at room temperature, to break the disulfide bonds.

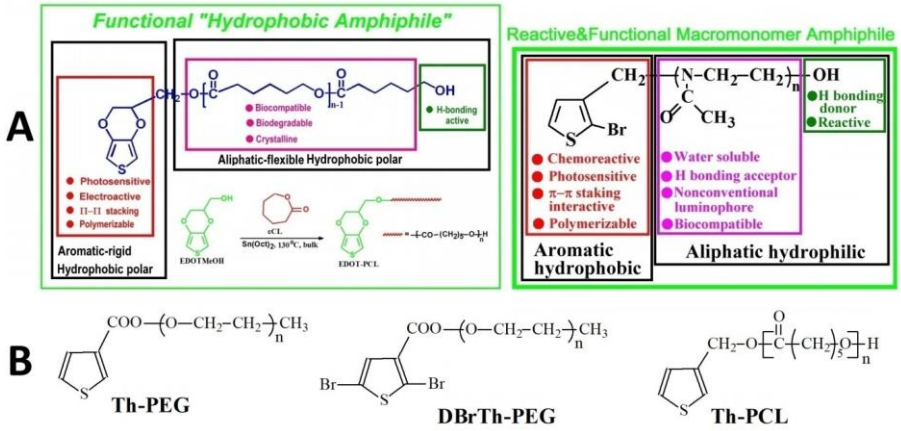

Figure 10. *(**A**) Design criteria for the construction of the thiophene-ring-containing electroactive macromonomers. (**B**) Other thiophene-containing macromonomers synthesized in the frame of 5DnanoP project.*

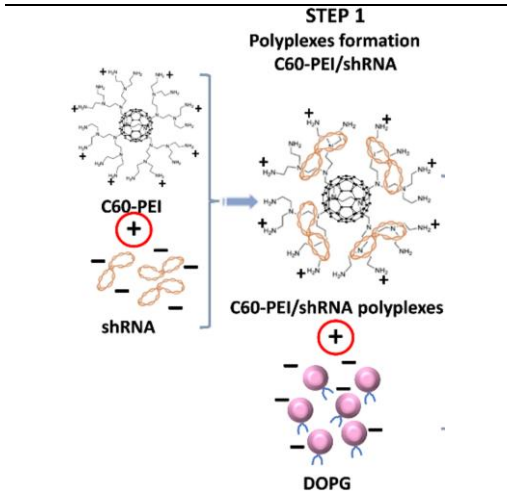

Figure 11. *Schematic representation of the successive steps in the synthesis of VCAM-1.*

The polyplexes are functional as they downregulate the Runx2 gene and protein expression, and their uptake leads to a significant decrease in the expression of osteogenic molecules (OSP, BSP, BMP-2). These results identify a new, appropriately directed vehicle that could be instrumental in developing novel strategies for blocking the progression of CAVD using a targeted nanomedicine approach.

5.2. Finalizing the procedures for obtaining and characterizing nanoplatforms

5.2.1. Structural characterization and properties investigations of the nanoplatforms constituents

The structural characterization and confirmation of the macromonomers anticipated structures were performed by usual spectroscopic methods basically by NMR (various techniques) and by FT-IR. GPC was employed for the molecular weight and index of the polydispersity evaluation. The properties in bulk very often were assessed by thermal methods as DSC and TGA methods. The properties in solution (aqueous or of organic nature) were investigated by dynamic light scattering (DLS), UV-vis and fluorescence spectroscopies, sometimes combined with particular 2D NMR techniques.

As an illustration of such applied techniques, in ***Figure 12.A***, ^{1}H-NMR spectra for Th-OMeOx are presented, measured in deuterated solvents with different polarities in order to accurately prove its structure and also its micellar self-assembled state. In ***Figure 12.B***, the fluorescence property of these formed micelles was demonstrated, which was triggered by a clusterization phenomenon of OMeOx in confined spaces of the micelles.

5.2.2. Strategies for nanoplatforms construction based on grafted conjugated electro-conducting polymers (g-CPs)

From the proposal stage, 5DnanoP project stated that the intended nanoplatforms with potential use in various types of biomedical therapy have to be constructed with brush-type spacers connected to a "substrata", which can be of macromolecular nature. Following the initial paradigm of the project, we used the above mentioned electroactive macromonomers to synthesize the model-proposed architecture by the "side chains first" approach; given the fact that it offers many advantages, the most important one being the possibility to exactly adjust the length of the side chains by manipulating the reaction conditions during the macromonomers synthesis. Two types of such nanoplatforms were obtained (**i**) molecular nanoplatforms for which "substrata" were conjugated electro-conducting chains and (**ii**) a macroscopic 3D hybrid bioplatform formed by a self-standing film of isotactic polypropylene (i-PP), (a synthetic polymer that is typically used for biomedical applications, e.g. fabrication of implants) and a nanostructured 9 μm thick superficial layer formed by a PEDOT-based g-CPs with PCL side chains.

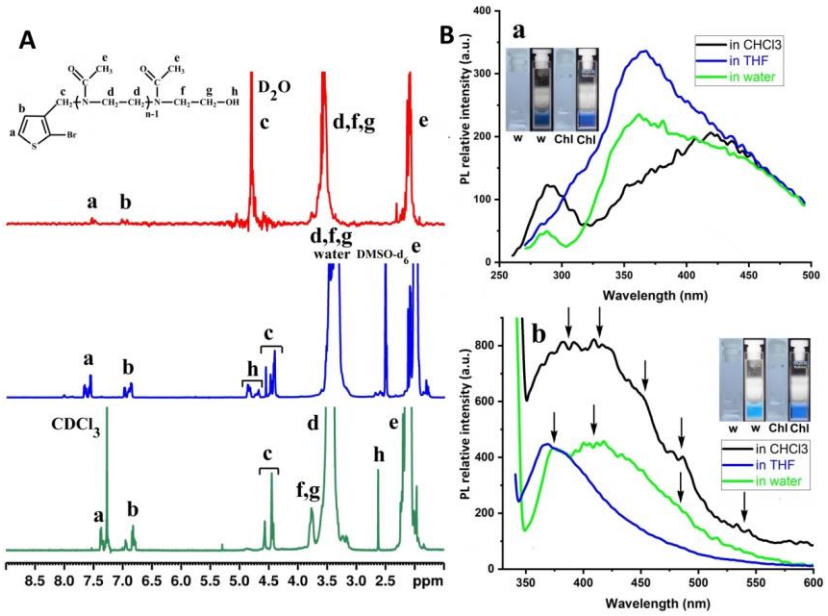

Figure 12. *Structural and properties characterization of thiophene-oligo(2-methyl-2-oxazoline) macromonomer (TH-OMeOx)(**A**)- by H-NMR spectroscopy and (**B**)- by fluorescence spectroscopy.*

I. Molecular nanoplatforms

The molecular nanoplatforms were synthesized by applying different methods of chemical polymerization. A random, heterografted amphiphilic polythiophene, containing biocompatible and biodegradable side chains (PEG and PCL) (***Figure 13***), was obtained by oxidative polymerization, catalysed by $FeCl_3$.

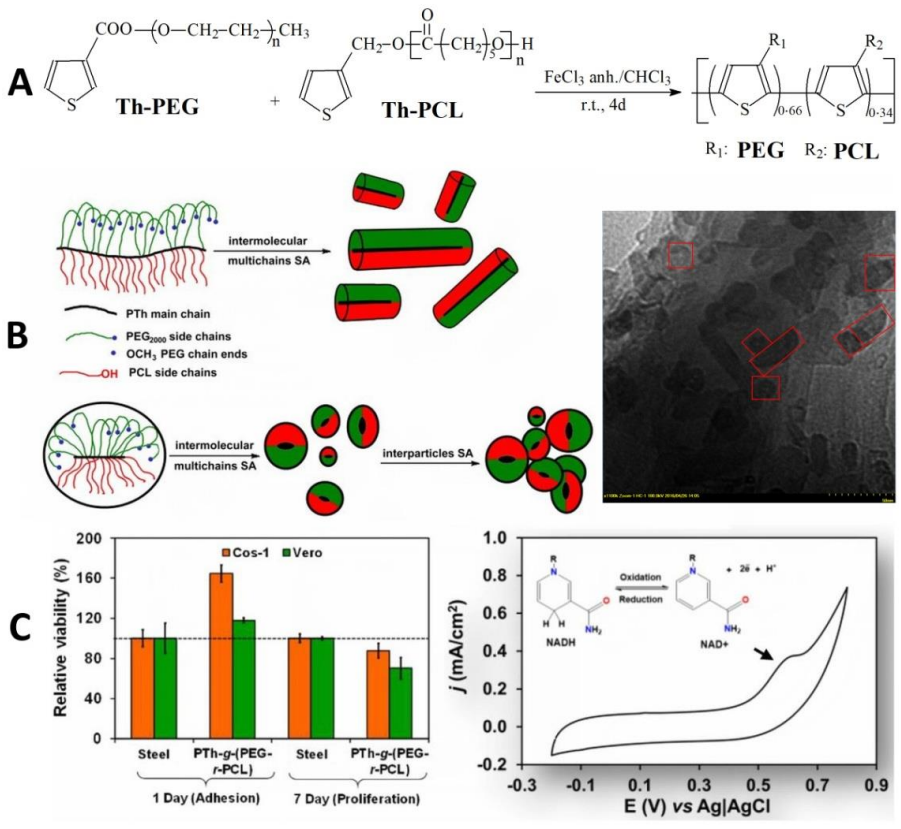

Figure 13. *(**A**)-Synthesis by chemical oxidative polymerization of an amphiphilic, heterografted polythiophene; (**B**)- Representation of the self-assembling of the copolymer in acetone solution and the TEM image of the supramolecular nano-objects formed in its thin film; (**C**)- (left)- Biocompatibility of copolymer in the presence of fibroblast (Cos-1) and epithelial (Vero) cell lines and (right)- the capability of the copolymer as an amperometric sensor for NADH coenzyme detection.*

In another attempt water-self dispersible thiophene-containing alternating copolymers were obtained by Suzuki polycondensation between a Th-PEG macromonomer and aromatic diboronic acids having the aromatic moiety of different sizes (***Figure 14.B***). The properties of the obtained copolymers can be tuned not only by the length of the side chains but also by modifying the side chains grafting

density by changing the size of the aromatic ring of the diboronic acid as is schematically illustrated in ***Figure 14.A***.

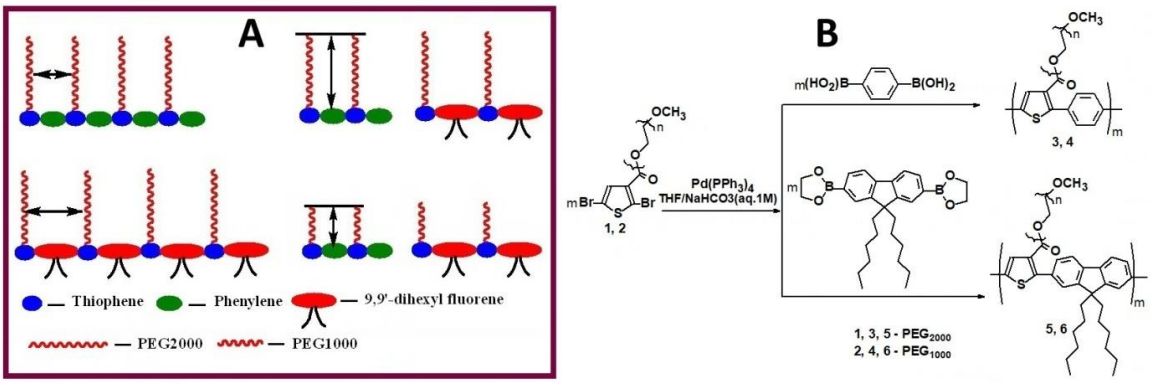

Figure 14. *(**A**)-Schematic representation of the adopted design criteria for synthesized fluorescent, water-self dispersible conjugated copolymers for the modulation of the micellar nanoplatforms' properties; (**B**)- Synthesis of water self-dispersible conjugated polymers synthesized by Suzuki polycondensation*

In another attempt a less commonly used polymerization method was applied, namely self-acid-assisted polymerization (SAAP) of a 2-bromo-substituted macromonomer Th-OMeOx (***Figure 15.A***). SAAP is an ideally attractive and environmentally sound procedure while requiring inexpensive and uncomplicated equipment. In spite of the fact that the reaction was not complete, most probable due to the macromonomer's chain slow mobility into the viscous system, the importance and novelty of our findings rely on the fact that, to the best of our knowledge, this is the first example of SAAP in the bulk of a 2-substituted thiophene compound which is not a crystalline one, enlarging in this way the thiophene-based SSP database.

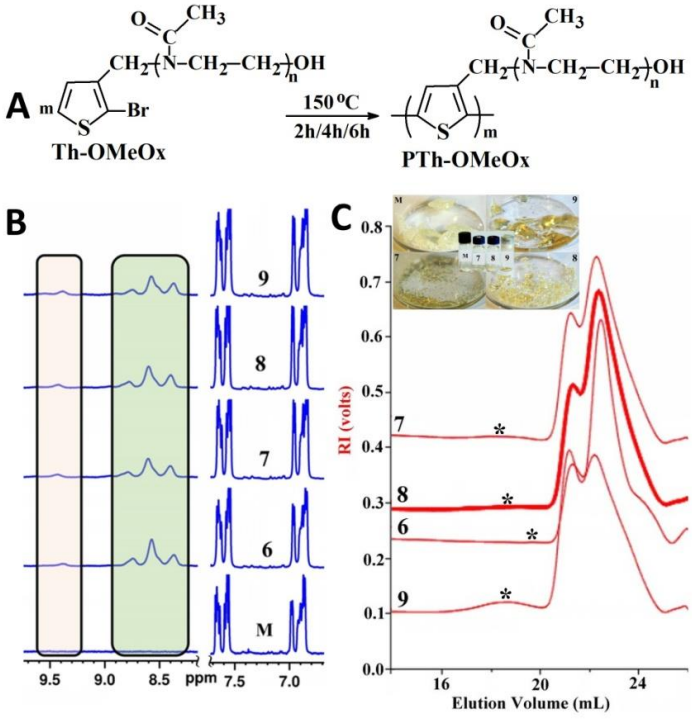

Figure 15.
*(**A**) Self-Acid Assisted Polymerization (SAAP) of Th-OMeOx macromonomer in bulk.*
*(**B**) ^{1}H-NMR characterization of the resulted mixture.*
*(**C**) GPC traces of the resulted mixtures for a different time- intervals of SAA polymerization of Th-OmeOx.*

II. Macroscopic-size hybrid bioplatform hierarchically structured at the nanoscopic level

The 3D bioplatform presented in ***Figure 16*** was constructed by combining the physical processes with the chemical ones, in a sequential manner.

Thus, in the first step, the functionalization of isotactic polypropylene was performed by applying a plasma treatment, followed by surface coating with a layer of polyhydroxymethy-3,4-

ethylenedioxythiophene nanoparticles (PHMeEDOT NPs) by in situ chemical oxidative polymerization of HMeEDOT.

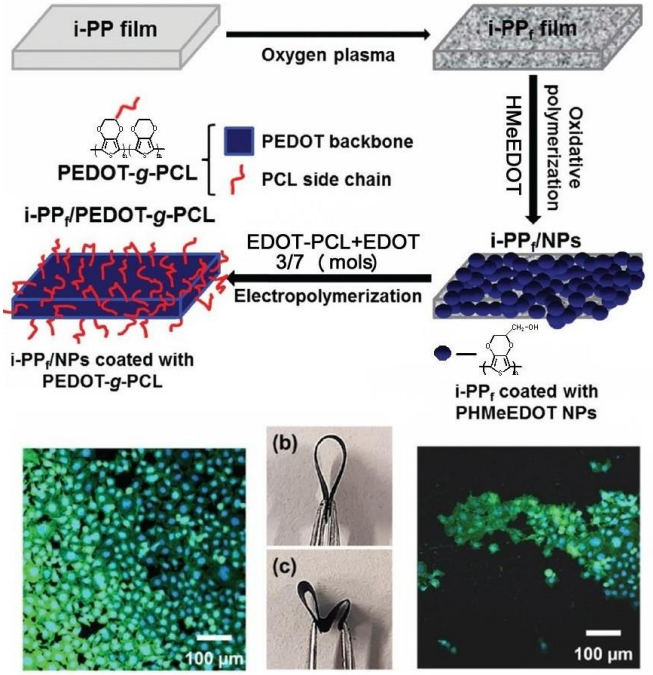

Figure 16. *The hierarchical strategy for the construction of nanostructures-containing macroscopic bioplatform and images showing its biocompatibility (confocal microscopy) and flexibility (conformability) properties.*

5.3. Finalization of protocols and procedures for obtaining and characterizing matrices for *ex vivo* testing of nanoplatforms

In order to make drug development less costly and more efficient, one of the strategies is to use model systems that mimic more closely the *in vivo* tumor. These surrogate tissues can measure *in vitro* the drug efficiency during the preclinical stages of drug development or can be used to study tumor biology in vitro by monitoring cancer cell proliferation, invasion, matrix remodeling, angiogenesis or metastasis The two most important systems used today for testing chemotherapeutics are conventional two-dimensional (2D) systems (cell monolayers obtained by culture in plastic flasks) and three-dimensional (3D) tumor culture including spheroids, cellular multilayers, matrix embedding cultures, bioreactors and microfluidic devices. Even if the cost and the complexity of 3D platforms have limited their adoption as an industry standard, their use for drug screening has significantly developed in the last years.

5.3.1. Protocol for synthesis and characterization of tissue surrogates based on thermosensitive and injectable poloxamer-*graft*-carboxymethyl pullulan hydrogel

Synthesis of the precursors

Synthesis of Monoamine Derivative of Poloxamer (MAPlx)

MAPlx derivative was prepared in two steps: In the first step, 4-nitrophenyl formate-derivatized poloxamer was synthesized by the reaction in dichloromethane of poloxamer (1 g; 0.397 mmol) with an excess of 1.25:1 equivalents of 4-nitrophenyl chloroformate, at room temperature, for 4 h. The intermediate was recovered by precipitation in petroleum ether and subsequently washed with petroleum ether. The product was dried in a vacuum for 24 h. In the second step, the intermediate (0.34 mmol) was reacted with an excess of 3:1 equivalents of ethylenediamine. The reaction took place at room temperature in dichloromethane for 24 h. Finally, the reaction mixture was precipitated in petroleum ether and washed with ethyl ether. The dry precipitate was redissolved in distilled water and dialyzed against distilled water (molecular weight cut-off 2000 g/mol) for 5 days. The purified product was recovered by lyophilization.

Synthesis of Carboxymethyl Pullulan (CMP)

In a round-bottom flask with two necks, 20 g of P and 0.060 g $NaBH_4$ were dissolved in 35 mL of pure water. To the resulting solution, 40 mL NaOH aqueous solution 38% (w/v) and 35 g of monochloroacetic

acid (MCA) (MCA/OH molar ratio 1/1) were added sequentially at 50 °C as follows: (i) 20 mL of NaOH aqueous solution and 17.5 g of MCA were added and the stirring continued at 50 °C for 1 h; (ii) 10 mL of NaOH aqueous solution and 8.75 g of MCA were added and the stirring continued for an additional 30 min; (iii) 10 mL of NaOH aqueous solution and 8.75 g of MCA were added, and the resulting solution was stirred at 50 °C for 24 h. After cooling at room temperature, the solution was dialyzed against distilled water (dialysis bag from Medicell International, England; molecular weight cut-off 12,000 g/mol) for 7 days, until the presence of chlorine ions in the washing water was no longer detected (by checking with $AgNO_3$ solution). The final product was recovered by freeze-drying (–57 °C, 5.5×10^{-4} mbar) using a lyophilizer ALPHA 1–2 LD Christ, Germany.

Synthesis of Grafted Copolymer (Plx-g-CMP) (*Figure 17*)

Over an aqueous solution of CMP (1%, w/v; 1.89 meq. COOH groups) acidified to pH = 3 with 0.1 N HCl, 0.12 mmol of EEDQ in methanol (1.5 mL) were dropwise added. The activated polysaccharide solution was then very slowly dripped at room temperature, over an aqueous solution of MAPlx (6%, w/v; 0.18 mmol). The reaction took place at room temperature for 24 h. Finally, the reaction mixture was dialyzed successively, firstly against distilled water/methanol mixture (4/1, v/v) for 3 days and then distilled water for 4 days (dialysis bag from Medicell International, England; molecular weight cut-off 12,000 g/mol). The final product was recovered by lyophilization for 48 h at –57 °C, and 5.5×10^{-4} mbar.

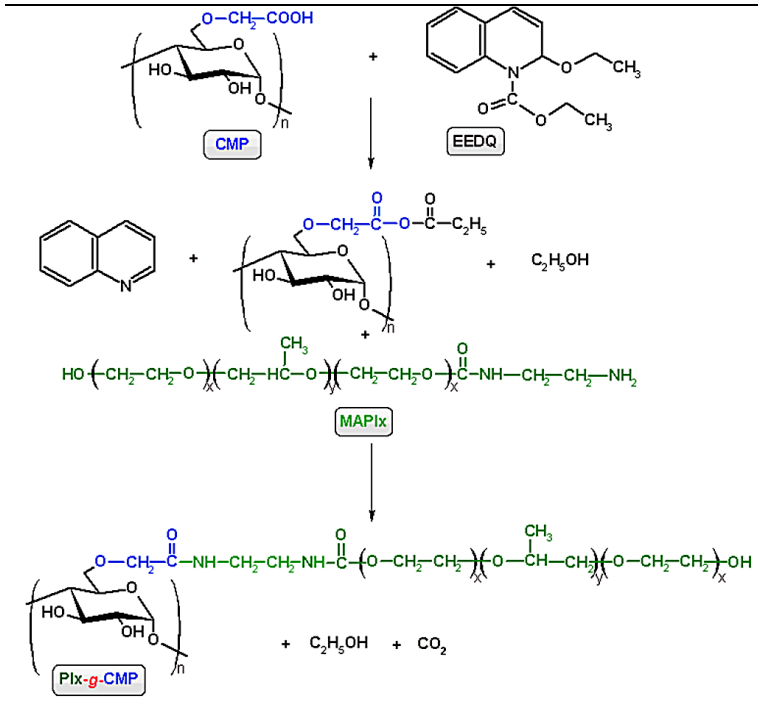

***Figure 17**. Synthesis route of Poloxamer-graft-carboxymethyl pullulan copolymer*

Characterization

Mn pullulan: 200,000 g/mol

Mn CMP (determined by GPC): 194,000 g/mol

Mw/Mn: 2.3

Degree of substitution of pullulan with CM: 29/100 sugar units

Degree of substitution of CMP with Plx: 10 mol% (mol of Plx/100 anhydroglycosidic unit of CMP)

IR n_{max} (KBr), cm^{-1}: 3435w, 2971m, 2890m, 2742m, 2695m, 1740s, 1619w, 1543m, 1469s, 1344s, 1282s, 1243s, 1149m, 1112s, 1061m, 963s, 842s, 758m, 671m, 579m, 529s, 509m

^{1}H NMR (D_2O, 400 MHz) δ (ppm): 5.524 (1H, $H_{1,4}$, CMP), 4.97 (1H, $H_{1,6}$, CMP), 4.6-3.5 (6H, H_2-H_6, CMP; 2H, O-CH_2-, CMP; 4H, -NH-(CH_2)$_2$-NH, ligand; 4H, -O-(CH_2)$_2$-, PEO; 1H, O-C*H*-, PPO; 2H, -CH-CH_2-, PPO)

^{13}C NMR (D_2O, 100 MHz) δ (ppm): 185 (C8, unprotonated, CMP), 180 (C8, CMP), 174 (C11, Plx), 100 (C1, CMP), 79 (C4, CMP), 75-60 ((C2-C7 (CMP), C9, C10 (ligand), a,b (PEO), c,e (PPO)), 63 (C1, CMP), 20 (d, PPO).

Gelation temperature: 33 °C at a concentration of 11% and 20 °C at a concentration of 18% (w/v) (***Figure18***).

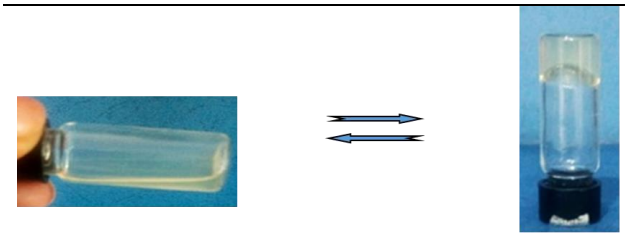

***Figure 18**. Schematic representation of sol–gel transition of the Plx-g-CMP solution*

Potential applications: a surrogate for bio-medical testing, surrogate for cartilages and soft tissue.

5.3.2. Protocol for synthesis and characterization of sponge-type hydrogels composed of hyaluronic acid and poly(methylvinylether-*alt*-maleic acid) as surrogates for bio-medical testing

Hydrogel synthesis

Aqueous solutions containing 1:1 weight ratios of HA and P(MVEaltMA) were mixed resulting a final concentration of 3%, w/w. Solutions were quickly frozen in liquid nitrogen and then freeze-dried for 48 h until all the water was sublimed. The resulting sponge–type samples were obtained in cylinder-like pieces. These samples were not cross-linked and therefore they were soluble in water. In order to obtain cross-linked hydrogels, the samples were subsequently placed in the oven for 12h at 80 °C. The schematic representation of the synthesis steps of the surrogate is given in ***Figure 19***.

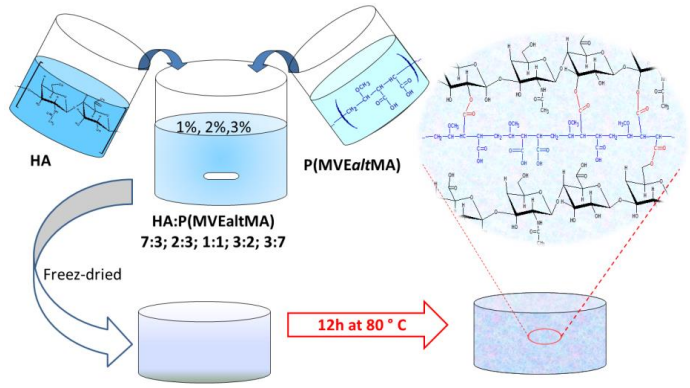

***Figure 19.** Schematic representation of the synthesis steps of sponge-type hydrogel*

Purification: The resulted cross-linked hydrogels were kept for 2-4 days in a large amount of water, frequently refreshed to remove the soluble fraction of polymer residues.

Recovery: Surrogates were recovered by frozen in liquid nitrogen and then freeze-dried for 48 h. The white solid scaffolds formed were cut into 2 mm × 2 mm × 1 mm pieces under a stereomicroscope (Zeiss, Oberkochen, Germany)

Sterilization: Samples were placed in a 24-well cell culture plate, and sterilized by UV exposure for 6 min.

Hydrogel characterization

SEM: Ordered and compact structure and large pores (d= 20-50 μm).

In a longitudinal section of hydrogels, the SEM micrograph indicated that the hydrogels present a lamellar structures arrangement, containing abundant pores between each layer, observable in cross-section (***Figure 20***).

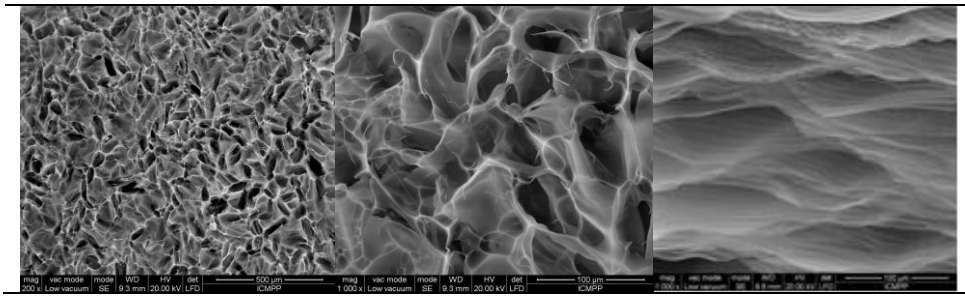

Figure 20. *Scanning electron micrographs of HA-P(MVEaltMA) surrogate*

IR ν_{max}, (ATR), cm^{-1}: 3386 (m), 2918 (m), 2890 (m), 1773 (m), 1849 (w), 1715 (s), 1641 (s), 1566 (m), 1078 (s), 1043 (s).

^{13}C CP-MAS NMR, δ(ppm): 176.20 (1C, -**C**OOH), 170.60 (1C, **C**OOR), 103.65 (1C, -**C**H-O-), 75.63 (5C, …-**C**H-**C**H-…), 68.05 (1C, -**C**H-CO), 57.48 (1C, -O**C**H_3), 43.56 (1C, -**C**H), 32,69 (1C, -**C**H_2), 23.48 (1C, -**C**H_3).

DSC: Endothermic peak at 168 °C reflecting the release of the bound water.
Two endothermic peaks at 203 and 236 °C which reflect the formation of both anhydride (between two COOH groups present in the P(MVE-alt-MA) chains) and ester bonds (between the COOH groups of P(MVE-alt-MA) and the OH groups of HA).

Exchange capacity: 2.45 ± 0.4 meq/g determined by conductometric titration

Swelling degree: 40.4 ± 2.1 w/w determined by difference between the weight of swollen hydrogels at equilibrium and the weight of dry hydrogels.

Cross-linking degree: 65.32 ± 1.9 (%) estimated from the difference between the theoretical exchange capacity and the effective exchange capacity determined by conductometric titration.

Drug loading: 525.39 ± 16.1 (mg/g) diphenhydramine (DPH); 436.69 ± 0.21(mg/g) lidocaine (Lid), 462.92 ± 23.14 (mg/g) propranolol (Prop)

Release studies: (***Figure 21***)

Potential applications: a surrogate for bio-medical testing, matrix for controlled drug delivery, polymeric support for cell culture

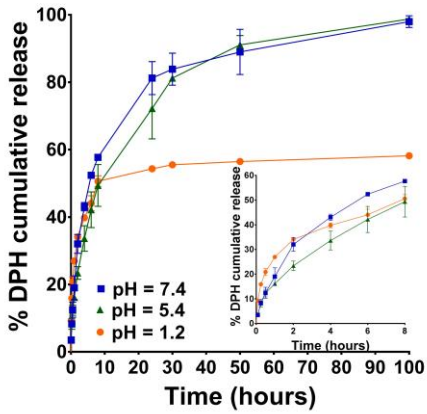

Figure 21. *Release profiles of DPH from HA-P(MVEaltMA) surrogate hydrogel at pH = 1.2, 5.4, and 7.4*

5.3.3. Protocols for testing the matrices' cytocompatibility and their use as tumor/tissue surrogates

The matrices (sponge-type hydrogels based on hyaluronic acid (HA) and poly (methyl vinyl ether-alt-maleic acid) were investigated using the optimized biological protocols described below. Based on the biological investigation data they were proposed as appropriate scaffolds to support cell growth and function as tissue/tumor surrogates for further ex vivo testing of nanoplatforms.

Cell culture

2D cell culture. HepG2 cells (American Type Culture Collection, Manassas, Virginia, USA) were grown in polystyrene cell culture plates using Dulbecco's Modified Eagle's Medium (DMEM) with 0.45% glucose, supplemented with 10% (v/v) fetal bovine serum (FBS), 100 units/mL penicillin, and 100

units/mL streptomycin and was maintained at 37 °C in an incubator with a 95% humidified atmosphere of 5% carbon dioxide in the air. For sub-culturing, cells were trypsinized using a 0.25% trypsin solution with 0.5 mM EDTA. HepG2 cells were seeded on 24- wells cell plates (diameter 15.6 mm) with a density of $2.5 \cdot 10^5$ cells/well.

3D cell culture. Pieces of hydrogel (approx. 2 × 2 × 1 mm) were cut under a stereomicroscope and then weighed and sterilized by exposure to UV radiation for 3 min on each side. Without any washing procedure, the hydrogels were populated with HepG2 cells at a cell density of $2.5 \cdot 10^5$ cells/3D support by spotting 10 μL of cell suspension.

Cytotoxicity evaluation

XTT assay (Colorimetric Assay). The viability of HepG2 cells grown in the HA-based hydrogels was investigated with the XTT colorimetric assay, following the conversion of 2,3-bis-(2-methoxy-4-nitro-5-sulfophenyl)-2H-tetrazolium-5-carboxanilide (XTT) into orange formazan by the metabolically-active cells in the presence of the reducing agent phenazine methosulfate (PMS). $2.5 \cdot 10^5$ HepG2 cells were added to hydrogels and 2D supports and incubated at 37 °C, for 1 day (D1, taken as the control), 7 days (D7), 14 days (D14), and 21 days (D21). At 24 h after seeding (D1), the hydrogels were relocated into new wells and the culture medium was refreshed every 2–3 days. Cell populated hydrogels were examined after medium replacement by light microscopy (ZEISS Microscope). At each experimental time point, cell-populated hydrogels and 2D supports were washed with PBS followed by incubation with a 250 μL mixture containing XTT (0.25 mg mL−1) and PMS (0.025 mM) in colorless DMEM, for 3 h at 37 °C. The intensity of the orange color of formazan in the medium was quantified spectrophotometrically by measuring the absorbance at 450 nm using a TECAN Infinite M200Pro (Tecan Group Ltd., Männedorf, Switzerland). The results were expressed as a percentage of values obtained from cells seeded on 2D supports incubated for 24 h (D1) and normalized to hydrogel and 2D, respectively.

ToxiLight cytotoxicity bioassay (Bioluminescent Assay). For cell toxicity assay, the highly sensitive bioluminescent, non-destructive assay kit (ToxiLight™ BioAssay Kit) is designed to measure the release of the enzyme, adenylate kinase (AK), from the cell supernatant of damaged cells. The AK levels were measured in the medium collected on the first day (D1) and day 21 (D21) after seeding of cells in the hydrogels and on the 24-well plates (2D supports) at a density of $2.5 \cdot 10^5$ HepG2 cells/hydrogel or 2D support. At each time point, the cells were subjected to radio immune-precipitation assay buffer (RIPA) lysis, sonicated, and centrifuged at 10.000 ×g, at 4 °C, for 10 min. The total protein content (mg/mL) was assessed by BCA colorimetric method and was used for normalization.

Live/dead viability/cytotoxicity assay (Fluorescent Assay). The same seeding density of cells ($2.5 \cdot 10^5$ cells) was used for hydrogel (3D) or 2D support. After culturing for 1 day and 21 days, the cells grown in both 3D and 2D were stained with a live/dead cell double staining kit accordingly to the manufacturer's instructions. Thus, viable cells are stained by calcein-AM, emitting a strong green fluorescence, whereas dead cells are stained by propidium iodide (PI) and emit red fluorescence. A Z-stack acquisition image series were recorded using the Inverted Microscope Olympus IX81 equipped with fluorescence filters to detect green and red fluorescence. The 3D reconstruction images were generated using Image J software (developed at the National Institutes of Health (NIH), USA) to give a 3D representation of cell viability and infiltration within the hydrogel.

Cell morphology examination. To evaluate the cell morphology of HepG2 cells grown for 21 days on plastic 2D support and in the developed HA-based scaffolds, fluorescence microscopy was employed. At each experimental time point, the cells grown in 2D and 3D culture systems were washed three times with PBS, fixed in 4% PFA in 0.1 M phosphate buffer (pH 7.4), permeabilized with 0.5% Triton X-100, and stained with 200 ng/mL phalloidin-FITC and 2 μg/mL DAPI. The samples' examination was performed with the 20× objective of the Inverted Microscope Olympus IX81 using the Z-stacking option of CellSens Dimension 1.5 software© Olympus Corporation (Shinjuku, Tokyo, Japan). Consecutive Z-stacks were acquired on a thickness of 90 μm, with a step size of 8.06 μm.

Statistical analysis. The experiments were performed at least in triplicate. All the results are reported as mean ± standard deviation. Statistical evaluation was carried out by unpaired Student's t-test (two-tailed) using the GraphPad Prism 7 software. Differences were considered statistically relevant when $p < 0.05$ and statistically highly relevant when $p < 0.001$.

Other five interpenetrated hydrogels based on hyaluronic acid (HA), poly(methyl vinyl ether-*alt*-maleic acid) (P), with or without thermosensitive polymer poly(N-isopropylacrylamide-*co*-N-hydroxyethylacrylamide) (HAIPN) were developed by partner P3. The codes of the 5 hydrogels were: HA30P, HA30IPN (1), HAIPN (2), HA50P, HAIPN3 (1), which differ in the concentration of polymers used to obtain them. The partner P5 performed the cytocompatibility investigations of these matrices

using human embryonic kidney cells, HEK293 cell line (ATCC) grown in a complete DMEM medium containing 4.5 ‰ glucose. The viability of HEK293 cells treated with the conditioned medium resulting from the incubation of 1 mg/mL hydrogel in complete DMEM for different time intervals (2, 6, 24, and 30 hours) was determined using the XTT assay. HEK293 cells were seeded in 96-well plates at a density of $7 \cdot 10^3$ cells/well and kept for 24 hours in an incubator with 5% CO_2 and 37°C. Then, the cells were treated for another 24 hours with the complete medium (control) or conditioned medium from the 5 hydrogels. At the end of the incubation interval, each well was incubated for 2 h at 37 °C with a 100 µL mixture of 0.25 mg/mL XTT and 1.87 µg/mL PMS in DMEM. Then, the absorbance at 450 nm was measured using the Tecan Infinite M200Pro microplate reader (Tecan Group Ltd., Switzerland). The results were reported on the data obtained for the untreated cells, control, considered to have a viability of 100% (***Figure 22***).

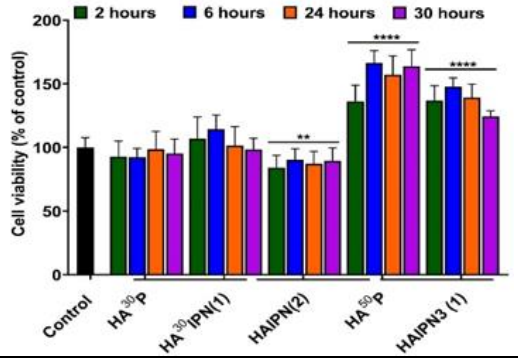

Figure 22. *Viability of HEK293 cells assessed by XTT test. Cells were treated for 24 hours with a conditioned medium from hydrogels incubated in complete DMEM (1 mg/mL) for 2, 6, 24, and 30 hours. Statistical significance: ** p <0.01, **** p <0.001 compared to control.*

These results suggest that the 5 hydrogels tested are biocompatible with living cells in culture and may be proposed as tissue surrogates or drug delivery platforms.

5.4. Finalization of protocols for testing the functionality of nanoplatforms

5.4.1. Protocols for testing nanocarriers for controlled delivery of antitumor drugs to cancer cells

Doxorubicin-loaded nanospheres (NS-DXR), consisting of pH-sensitive poly (N-isopropyl-acrylamide-*co*-vinylimidazole) copolymer, synthesized by the partner P3 were characterized in vitro and tested in vivo by the partner P5. For this, their ability to transport encapsulated DXR to tumor tissues was studied. Thus, two human tumor cell lines were used, liver carcinoma cells (HepG2) and lung adenocarcinoma cells (A549). Hemolysis and aggregation of ex vivo erythrocytes induced by NS-DXR were also studied. To study the in vivo distribution and pharmacokinetics of NS-DXR, NS-DXR was administered to C57BL/6J mice and the results were compared to mice injected with free DXR or untreated mice (injected with the phosphate-buffered solution, PBS).

Cell culture

The human hepatocellular carcinoma (HepG2) cell line was grown in DMEM containing 4.5 ‰ glucose, while the human alveolar basal epithelial cell line of human adenocarcinoma (A549) was cultured in DMEM-containing 1‰ glucose. The DMEM media was supplemented with 10% fetal bovine serum (FBS, Sigma-Aldrich, Germany) and 1% antibiotics (100 U/mL penicillin and 100 µg/mL streptomycin) to form complete culture media. Cells cultured in these complete media were maintained in cell culture plates in an incubator at 37°C and 5% CO_2.

In vitro cytotoxicity analysis

XTT assay (Colorimetric Assay). The effect of different concentrations of free DXR, NS-DXR or NS on cell viability was evaluated using XTT reagent. HepG2 and A549 cells were seeded for 48 h at a density of 104 cells/well on flat-bottom 96-well plates and incubated with various concentrations of NS or NS-DXR (3.9 ÷ 125 µg/mL) and free DXR, at the corresponding concentrations as entrapped into MS-DXR (0.078 ÷ 2.5 µg/mL) for 24 h. At the end of the incubation interval, each well was incubated for 2 h at 37 °C with 100 µL mixture of 0.25 mg / mL XTT and 1.87 µg / mL PMS in DMEM. Then, the absorbance at 450 nm was measured using the Tecan Infinite M200Pro microplate reader. Cell viability was expressed as % of untreated cells (control) considered 100% viable. The IC50 (half maximal inhibitory concentration, namely the concentration of a cytotoxic compound that induces 50% inhibition of the cell proliferation) was determined by plotting the percentage of cell growth inhibition versus the compound concentration.

ToxiLight cytotoxicity bioassay (Bioluminescent Assay). The cytotoxicity induced by the exposure of HepG2 and A549 cells to different concentrations of free DXR, NS-DXR, or plain NS (identical concentration of nanospheres as NS-DXR, but without DXR) was determined using the ToxiLight assay kit. The assay uses luminescent detection to measure the levels of adenylate kinase (AK) released by the damaged cells into the culture media. HepG2 and A459 cells were seeded in a 96-well culture plate at a density of 104 cells/well and after 48 h the cells were treated with various concentrations of NS or NS-DXR (3.9 ÷ 125 μg/mL) and free DXR, at the corresponding concentrations as entrapped into NS-DXR (0.078 ÷ 2.5 μg/mL) for 24 h. Then, the culture medium was collected, and the cytotoxicity was assessed using the bioluminescent kit according to the manufacturer's instructions. The results were expressed as fold change relative to the results obtained for the untreated control cells.

In Vitro Cellular Uptake of NS-DXR by Tumor Cells

Based on the fluorescent properties of DXR, the internalization of nanospheres loaded with DXR by two cancer cell lines (HepG2 and A549 cells) was investigated by fluorescence microscopy. Cellular uptake of NS-DXR compared to free DXR was determined by treating HepG2 and A459 cells with two concentrations of DXR (1.25 and 2.5 μg/mL), either free or loaded into NS-DXR. For both cell lines, 104 cells were grown for 48 h on a 96-well culture plate. Then, the cells were incubated for 6 and 24 h at 37 °C with NS-DXR or free DXR in a complete medium. Cells were then washed with phosphate-buffered saline (PBS), fixed with 4% paraformaldehyde (PFA), stained with 100 ng/mL phalloidin-FITC (Bio-Techne Ltd., Minneapolis, MN, USA) for actin cytoskeleton and 2 μg/mL 4′,6-diamidino-2-phenylindole (DAPI, ThermoFisher Scientific) for cell nuclei. The intracellular localization of DXR after incubation of the cells to NS-DXR or free DXR was examined with the Inverted Microscope Olympus IX81 (40× magnification objective), and the representative images were taken using the following filter cubes: U-MNG2 filter, λ excitation/emission: 555/580 nm to detect DXR-derived red fluorescence; U-MNU2 filter, λ excitation/emission: 345/478 nm to detect the DAPI-derived blue fluorescence; and U-MNB2 filter, λ excitation/emission: 494/518 nm to detect FITC-derived green fluorescence.

Animals

Sixteen-week-old male C57BL/6J mice (Stock No: 000664) from The Jackson Laboratory (Bar Habor, ME, USA) were used to investigate the hemocompatibility and the biodistribution of NS-DXR compared to free DXR. Mice were kept in a specific pathogen-free facility at 24 °C in a temperature-controlled chamber with a 12 h light/dark cycle and had access to a standard rodent diet and water ad libitum.

In Vitro Hemocompatibility Test

To evaluate the blood compatibility of NS-DXR compared to plain NS and free DXR, the hemolysis was investigated as previously reported. The erythrocytes were isolated from the blood collected in EDTA tubes by cardiac puncture from C57BL6J mice. The blood samples were centrifuged for 15 min, at 1000×g and 4 °C, and the plasma was carefully separated, pooled, and stored at 20 °C for further analysis. The erythrocyte mass was pooled and incubated at a 1:10 ratio in PBS containing different concentrations of NS and NS-DXR (ranging from 0.0078 to 1 mg/mL) or the corresponding free DXR (0.156–20 μg/mL). After incubation for 1 h, on an orbital shaker at 37 °C (OHAUS, Parsippany, NJ, USA), the samples were centrifuged to sediment the intact erythrocytes, and the hemoglobin released in the supernatants was measured at 540 nm with a TECAN Infinite M200Pro plate reader. As the negative control, the erythrocytes incubated with PBS were used, while the positive control (100% hemolysis) was obtained by the erythrocyte's incubation with 0.5% Triton X-100 (TX-100).

In Vivo Biodistribution and Hemocompatibility Studies

The C57BL6 mice received a retro-orbital injection of NS-DXR (150 mg NS/3 mg DXR/kg body weight, n = 4 mice) and free DXR (3 mg DXR/kg body weight, n = 3 mice) or PBS (as control for fluorescence background, n = 2 mice). At 1 h after administration, the mice were anesthetized with ketamine/xylazine and the blood was collected by cardiac puncture. To remove blood, perfusion through the left ventricle with PBS containing Ca^{2+} and Mg^{2+} was performed. The urine samples were collected from the mouse bladder. The brain, lungs, heart, liver, spleen, and kidneys were harvested and the DXR fluorescence was examined by ex vivo imaging, using the IVIS Spectrum Caliper 200 system with excitation/emission filter pairs: 500 nm/600 nm. For the spectral unmixing option, to discriminate between tissue autofluorescence and DXR fluorescence, the following excitation/emission filter pairs: 500 nm/580 nm, 500 nm/600 nm, 500 nm/620 nm, and 500 nm/640 nm were used. The fluorescent radiant efficiency [fluorescence emission radiance per incident excitation intensity $(p/sec/cm^2/sr)/(\mu W/cm^2)$] of DXR was quantified using the region of interest (ROI) option of Living Image 4.3.1 software and the resulting intensities were reported to the corresponding organ weight (g).

Additionally, the DXR concentration was measured in plasma and urine samples, using a validated fluorescent quantitative method. Briefly, 50 µL of undiluted plasma sample or 50 µL of urine (diluted in PBS at a 1:4 ratio) were added to a black 96-well plate. The fluorescence intensity of DXR in the plasma and urine samples was measured using the TECAN Infinite M200Pro, at λ_{ex} 480 nm and λ_{em} 590 nm. A standard curve of known DXR concentrations (0.625 ÷ 20 µg/mL) was used to determine the concentration of DXR in plasma and urine. In addition, the erythrocytes isolated from mice treated with NS-DXR and DXR were investigated for aggregation by light microscopy. Images were taken using the 40× objective of the Olympus IX81 Microscope.

RESULTS

Evaluation of cytotoxicity of NS-DXR nanospheres. Both methods have shown that the viability of HepG2 and A549 cells was not affected by the incubation with unloaded NS (***Figure 23***). This result suggests the cytocompatibility of NS with tested cell lines. Moreover, HepG2 and A549 cells show different sensitivities towards NS-DXR and free DXR.

In Vitro Cellular Uptake of NS-DXR. The accumulation of NS-DXR particles and free DXR in HepG2 and A549 cells was investigated using fluorescence microscopy (***Figure 24***). The fluorescence images revealed that both NS-DXR and free DXR were internalized by the cells in a dose- and time-dependent manner. It can be observed that DXR is mainly localized in the nuclei of HepG2 and A549 cells, consistent with previous studies comprising other DXR-delivery systems.

In Vitro Hemocompatibility. As a preliminary step toward the further preclinical investigation of the therapeutic potential of NS-DXR in animal models after intravenous administration, we assessed the hemolytic behavior of NS, NS-DXR, and free DXR. The results (***Figure 25***) showed that the percentage of hemolysis did not exceed 3.5%, pointing out that the erythrocytes were not affected by the incubation with NS, NS-DXR, and free DXR. A threshold of 5% hemolysis is considered acceptable for biomaterials, according to International Organization for Standardization (ISO) 10993-4:2017.

In vivo Biodistribution and Hemocompatibility of NS-DXR. The localization of NS-DXR and free DXR in different organs, after retro-orbital injection in C57BL6 mice, was investigated by fluorescent optical imaging, based on DXR's fluorescent properties (see ***Figure 26***). Thus, one hour after NS-DXR, free DXR, or PBS administration, the blood was drawn by cardiac puncture and, after thoroughly washing of the vasculature with PBS through the left ventricle, the organs (brain, lungs, heart, liver, spleen, kidneys) were harvested.

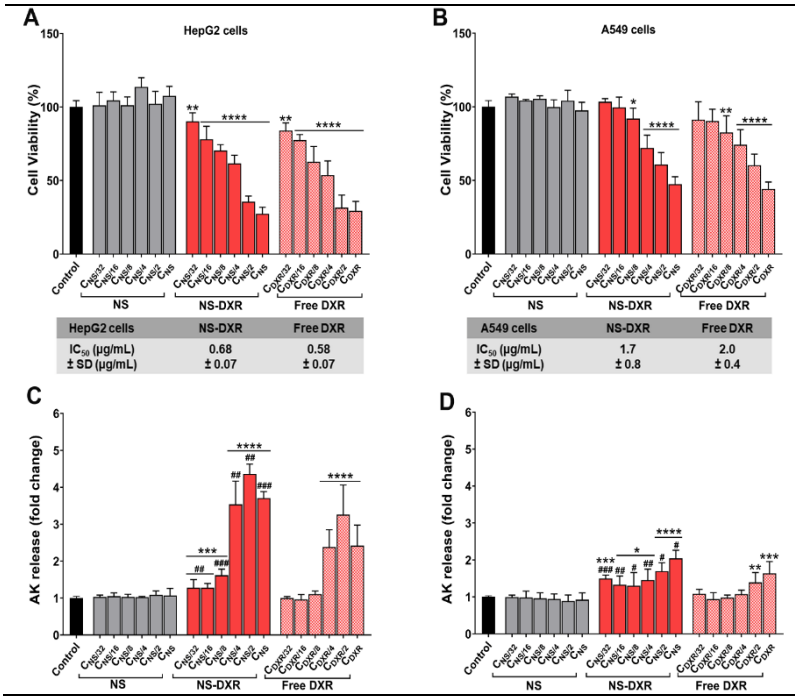

Figure 23. *The viability of HepG2 (A) and A549 (B) cells after exposure to plain NS, NS-DXR, and free DXR determined by XTT assay. The cytotoxicity of plain NS, NS-DXR, and free DXR on HepG2 (C) and A549 (D) cells determined by ToxiLightTM assay. Cells were exposed for 24 h to various concentrations of NS and NS-DXR (3.9 ÷125 µg/mL, CNS = 125 µg/mL) and the corresponding concentrations of free DXR (0.078 ÷ 2.5 µg/mL, CDXR = 2.5 µg/mL). Results are expressed as means ± standard deviation (S.D.) of three experiments performed at least in triplicates. * p < 0.05, ** p < 0.01, *** p < 0.00, **** p < 0.0001 vs. control; # p < 0.05, ## p < 0.01, ### p < 0.001 vs. free DXR.*

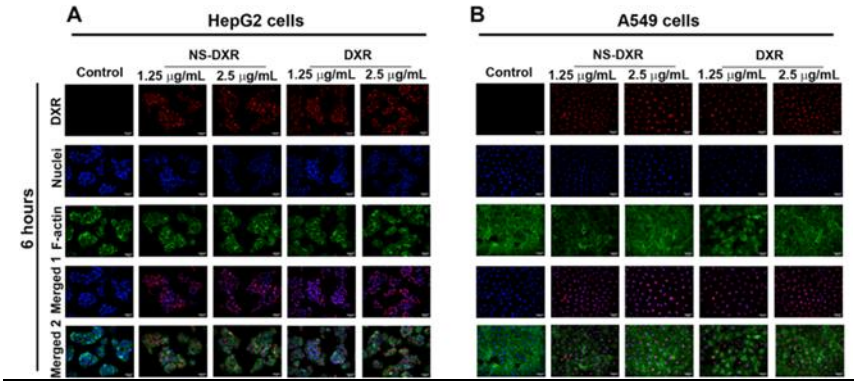

Figure 24. *DXR fluorescence was visualized in HepG2 (A) and A549 cells (C). Representative fluorescence microscopy images show the internalized DXR (red), nuclei stained by DAPI (blue) and F-actin, obtained by cell staining with FITC-labeled phalloidin (green).*
Scale bar: 50 μm.

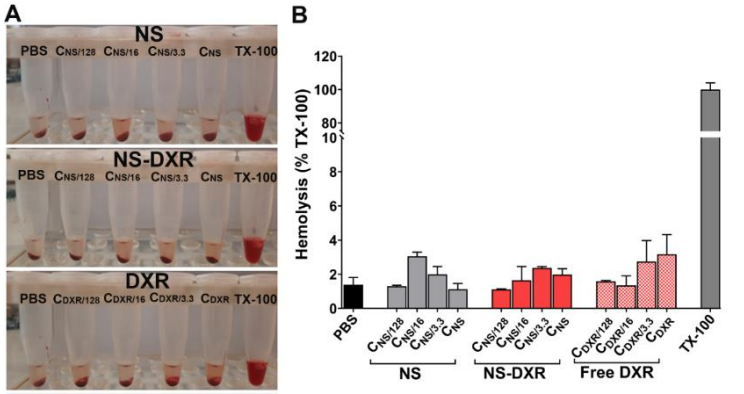

Figure 25. *In vitro hemocompatibility evaluation of NS, NS-DXR, and DXR. (A) Photographs of the sedimented erythrocytes after their exposure to various concentrations of NS and NS-DXR, and to the corresponding free DXR concentrations.(B) Quantification of hemolysis by measuring the absorbance of hemoglobin at 540 nm. Results are expressed as means ± standard deviation (S.D.) of one experiment performed in duplicate.*

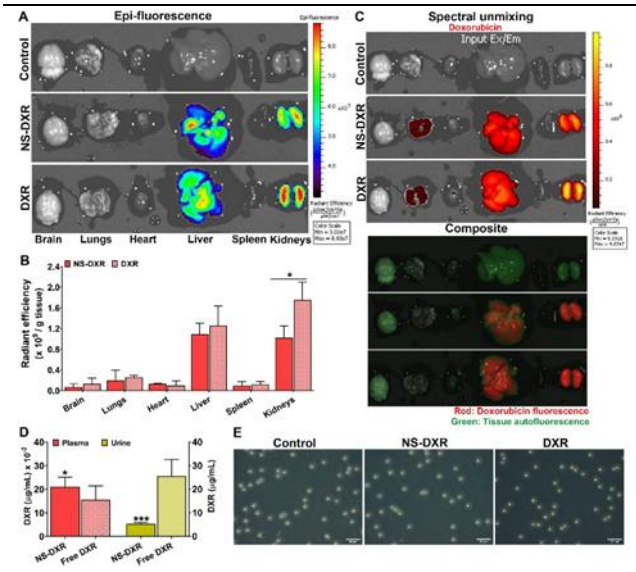

Figure 26. ***(A)*** *Localization of NS-DXR and free DXR in organs harvested from C57BL/6 mice. The analysis was completed 1 h after the retro-orbital injection of NS-DXR , free DXR, or PBS in mice using the imaging system IVIS Caliper 200, by detection of the DXR fluorescence using the filter set λex/λem: 500 nm/600 nm. (**B**) Quantification of total radiant efficiency in organs using the region-of-interest option of Living Image software. (**C**) Spectral unmixing analysis to delineate the signal specific for DXR fluorescence (red) and tissue autofluorescence (green). (**D**) Quantification of DXR in plasma and urine of mice, 1 h after administration of 3 mg/kg of free DXR or incorporated into NS-DXR, at λex = 480 nm and λem = 590 nm. * p < 0.05, *** p < 0.001. (E) Scale bar: 50 μm.*

5.4.2. Characterization techniques used for the bio-electroactive nanoplatforms

For the structural characterization of the obtained bio-electroactive nanoplatforms the same type of technical measurements as those for electroactive macromonomers was generally used (NMR, FT-IR), with the most important DEPT variants of ^{13}C-NMR applied when necessary. In ***Figure 15.B*** and C are given the ^{1}H-NMR spectra of the mixture containing poly/or oligomers of Th-OMeOx polymerised by SAA method by various time periods and the GPC traces of the same mixture, showing the development of the reaction. The fluorescence property was evaluated in solution of dispersion of the synthesized copolymers, while the size of the self-assembled supramolecular structures formed in selective solvents were assessed by DLS. A scenario of such kind of self assembling in acetone for the heterografted random polythiophene with PEG and PCL side chain is shown in ***Figure 13.B*** (left side), while the mixed morphology in thin film obtained by drop-casting the same solution was evidenced by transmission electron microscopy (TEM). Besides this technique also atom force microscopy (AFM) and scanning electron microscopy were used for morphology evaluation, as well.

The capability of the heterografted polythiophene to ideally work into aqueous electrolytes was evidenced by electrochemical methods. In ***Figure 13.C*** left side is presented the cyclic voltammogram of copolymer thin film deposited on a glassy carbon electrode with a peak characterizing the oxidation of NADH to NAD^+.
The biocompatibility of the bioplatform was evaluated by cell adhesion and proliferation in the presence of various cell lines. The results can be expressed as diagrams as that from ***Figure 13.C*** (left side) or by confocal microscopy micrographs displaying the morphology of cells as shown in ***Figure 16*** bottom line.

Dissemination of the results obtained during stage 2022 of 5D-nanoP project

***In parvo*:** 28 papers published in ISI ranked journals, 1 book chapter, 12 oral/poster communications, 2 keynote conferences, two meetings between partners (online), a final workshop (online), and 1 research stay.

Articles published in ISI journals with acknowledgments at the 5D-nanoP project (min. 5)

1. F. Mocci, L. Engelbrecht, C. Olla, A. Cappai, M.F. Casula, C. Melis, L. Stagi, A. Laaksonen, C. Maria Carbonaro, Carbon nanodots from *in silico* perspective, *Chemical Reviews*, Accepted (2022) (IF: 72.087)
2. Y. Dong, M. Gong, F. Ullah Shah, A. Laaksonen, R. An, X. Ji, Phosphonium-based ionic liquid significantly enhances SERS of cytochrome c on TiO2 nanotube arrays, *ACS Applied Materials & Interfaces* 14(23), 27456-27465 (2022). DOI: https://doi.org/10.1021/acsami.2c05781 (IF: 10.383)
3. Y. Dong, A. Laaksonen, M. Gong, R. An, X. Ji, Selective separation of highly similar proteins on ionic liquid-loaded mesoporous TiO2, *Langmuir* 38, 3202-3211 (2022). DOI: https://doi.org/10.1021/acs.langmuir.1c03277 (IF: 4.331)
4. Z. Zhang, T. Vasiliu, F. Li, A. Laaksonen, X. Zhang, F. Mocci, X. Ji, Novel artificial ionic cofactors for efficient electro-enzymatic conversion of CO2 to formic acid, *Journal of CO2 Utilization* 60, 101978 (2022). DOI: https://doi.org/10.1016/j.jcou.2022.101978 (IF: 8.321)
5. Y. Dong, W. Lin, A. Laaksonen, X. Ji, Complementary powerful techniques for investigating the interactions of proteins with porous TiO2 and its hybrid materials: A tutorial review, *Membranes* 12, 415 (2022). DOI: https://doi.org/10.3390/membranes12040415 (IF: 4.562)
6. F. Li, A. Laaksonen, X. Zhang, X. Ji, Rotten eggs revaluated: Ionic liquids and deep eutectic solvents for removal and utilization of hydrogen sulfide, *Industrial & Engineering Chemistry Research* 61, 2643-2671 (2022). DOI: https://doi.org/10.1021/acs.iecr.1c04142 (IF: 4.326)
7. Y. Wei, Z. Dai, Y. Dong, A. Filippov, X. Ji, A. Laaksonen, F. Ullah Shah, R. An, H. Fuchs, Molecular interactions of ionic liquids with SiO2 surfaces determined from colloid probe atomic force microscopy, *Physical Chemistry Chemical Physics* 24, 12808-12815 (2022). DOI: https://doi.org/10.1039/d2cp00483f (IF: 3.945)
8. Y. Wei, Y. Dong, X. Ji, F. Ullah Shah, A. Laaksonen, R. An, K. Riehemann, Detailing molecular interactions of ionic liquids with charged SiO2 surfaces: A systematic AFM study, *Journal of Molecular Liquids* 350, 118506 (2022). DOI: https://doi.org/10.1016/j.molliq.2022.118506 (IF: 6.633)
9. T. Vasiliu, F. Mocci, A. Laaksonen, L. De Villiers Engelbrecht, S. Perepelytsya, Caging polycations: Effect of increasing confinement on the modes of interaction of spermidine3+ with DNA double helices, *Frontiers in Chemistry* 10, 836994 (2022). DOI: https://doi.org/10.3389/fchem.2022.836994 (IF: 5.545)
10. L. Engelbrecht, X. Ji, Carlo M. Carbonaro, A. Laaksonen, F. Mocci, Excess molar enthalpies of pseudo-binary mixtures of a choline chloride-based deep eutectic solvent with water or methanol: An MD computer simulation study, Submitted to*: Frontiers in Chemistry* (2022). (IF: 5.545)
11. A.R. Petrovici, M. Silion, N. Simionescu, R. Kallala, M. Pinteala, S.S. Maier, Quantification of low amounts of zoledronic acid by HPLC-ESI-MS analysis: Method development and validation, *International Journal of Molecular Sciences* 23, 5944 (2022). DOI: https://doi.org/10.3390/ijms23115944 (IF: 6.208)
12. G. Voicu, D. Rebleanu, C.A. Mocanu, G. Tanko, I. Droc, C.M. Uritu, M. Pinteala, I. Manduteanu, M. Simionescu, M. Calin, VCAM-1 targeted lipopolyplexes as vehicles for efficient delivery of shRNA-Runx2 to osteoblast-differentiated valvular interstitial cells; Implications in calcific valve disease treatment, *International Journal of Molecular Sciences* 23, 3824 (2022). DOI: https://doi.org/10.3390/ijms23073824 (IF: 6.208)
13. A. Angeli, V. Kartsev, A. Petrou, B. Lichitsky, A. Komogortsev, M. Pinteala, A. Geronikaki, C.T. Supuran, Pyrazolo[4,3-c]pyridine sulfonamides as Carbonic Anhydrase inhibitors: Synthesis, biological and *in silico* studies, *Pharmaceuticals*, 15, 316 (2022). DOI: https://doi.org/10.3390/ph15030316 (IF: 5.215)
14. O.E. Carp, M. Pinteala, A. Arvinte, Innovative non-enzymatic electrochemical quantification of cholesterol, *Sensors* 22, 828 (2022). DOI: https://doi.org/10.3390/s22030828 (IF: 3.847)
15. G. Fundueanu, M. Constantin, M. Turtoi, S. Bucatariu, B. Cosman, M. Anghelache, G. Voicu, M. Calin, Bio-responsive carriers for controlled delivery of doxorubicin to cancer cells, *Pharmaceutics* 14, 865 (2022). DOI: https://doi.org/10.3390/pharmaceutics14040865 (IF: 6.525)

16. M. Constantin, B. Cosman, P. Ascenzi, B.C. Simionescu, G. Fundueanu, New chromatographic insights on drug: cyclodextrin inclusion complexes and their potential use in drug delivery, *International Journal of Biological Macromolecules*, Submitted (2022). (IF: 8.025)
17. C. Racles, M.F. Zaltariov, D. Peptanariu, T. Vasiliu, M. Cazacu, Functionalized mesoporous silica as doxorubicin carriers and cytotoxicity boosters, *Nanomaterials* 12, 1823, (2022). DOI: https://doi.org/10.3390/nano12111823 (IF: 5.719)
18. M. Turtoi, M. Anghelache, A.A. Patrascu, M. Deleanu, G. Voicu, M. Raduca, F. Safciuc, I. Manduteanu, M. Calin, D.-L. Popescu, Antitumor properties of a new macrocyclic tetranuclear oxidovanadium(V) complex with 3-methoxysalicylidenvaline ligand, *Biomedicines* 10, 1217 (2022). DOI: https://doi.org/10.3390/biomedicines10061217 (IF: 4.757)
19. B.I. Ciubotaru, M.F. Zaltariov, C. Tugui, I.E. Stoleru, D. Peptanariu, G.T. Stiubianu, N. Vornicu, M. Cazacu, Silicones with different crosslinking patterns: assessment from the perspective of their suitability for biomaterials, *Surfaces and Interfaces*, Accepted (2022) (IF: 6.137)
20. M.F. Zaltariov, M. Turtoi, D. Peptanariu, A.M. Macsim, L. Clima, C. Cojocaru, N. Vornicu, B.I. Ciubotaru, A. Bargan, M. Calin, M. Cazacu, Organosilatrane hanging 5-nitrosalicylaldimine motif: synthesis, full structural characterization and a multi-tool approach to assessing its medicinal significance, *European Journal of Medicinal Chemistry*, Under review (2022) (IF: 7.088)
21. A.-D. Bendrea, L. Cianga, G.L. Ailiesei, D. Goen-Colak, I. Popescu, I. Cianga, Thiophene α-chain-end - functionalized oligo(2-methyl-2-oxazoline) as precursor amphiphilic macromonomer for grafted conjugated oligomers / polymers and as a multifunctional material with relevant properties for biomedical applications, *International Journal of Molecular Sciences*, Accepted (2022) (IF: 6.208)
22. S. Cibotaru, V. Nastasa, A.-I. Sandu, A.-C. Bostanaru, M. Mares, L. Marin, Pegylation of phenothiazine – A synthetic route towards potent anticancer drugs, *Journal of Advanced Research* 37, 279-290 (2022). DOI: https://doi.org/10.1016/j.jare.2021.07.003 (IF: 12.822)
23. C. Stavarache, A. Nicolescu, C. Duduianu, G. L. Ailiesei, M. Balan-Porcarasu, M. Cristea, A.-M. Macsim, O. Popa, C. Stavarache, A. Hirtopeanu, L. Barbes, R. Stan, H. Iovu, C. Deleanu, A real-life reproducibility assessment for NMR metabolomics, *Diagnostics* 12, 559 (2022). DOI: https://doi.org/10.3390/diagnostics12030559 (IF: 3.992)
24. E. Papadopoulou, A. Nicolescu, L.S. Haug, T. Husøy, C. Deleanu, H. Dirven, B. Lindeman, Lipoprotein profiles associated with exposure to poly- and perfluoroalkyl substances (PFASs) in the EuroMix human biomonitoring study, *Environmental Pollution*, In Press / Early View (2022). DOI: https://doi.org/10.1016/j.envpol.2022.119664 (IF: 9.988)
25. L.-A. Stanciulescu, A. Scafa, C. Duduianu, R. Stan, A. Nicolescu, C. Deleanu, M. Dorobanțu, Lipoprofiling assessed by NMR spectroscopy in patients with acute coronary syndromes. Is the need for fasting prior to sampling?, *Diagnostics*, Accepted (2022) (IF: 3.992)
26. F.L. Barroso da Silva, C. Corrêa Giron, A. Laaksonen, Electrostatic features for the receptor binding domain of SARS-COV-2 wildtype and its variants. Compass to the severity of the future variants with the charge-rule, BioRxiv, June 17, 2022 - https://doi.org/10.1101/2022.06.16.496458 - To be published in *Journal of Physical Chemistry B* (IF: 3.466)
27. A. Neamtu, F. Mocci, A. Laaksonen, F.L. Barroso da Silva, Towards an optimal monoclonal antibody with higher binding affinity to the receptor-binding domain of SARS-CoV-2 spike proteins from different variants, BioRxiv Jan 5, 2022, 1-59. DOI: https://doi.org/10.1101/2022.01.04.474958 - To be published in *RSC Medicinal Chemistry* (IF: 3.47)
28. C. Correa Giron, A. Laaksonen, F.L. Barroso da Silva, Differences between Omicron SARS-CoV-2 RBD and other variants in their ability to interact with cell receptors and monoclonal antibodies, BioRxiv, Jan 31 2022, 1-69. DOI: https://doi.org/10.1101/2022.01.29.478316 - To be published in *Journal of Biomolecular Structure & Dynamics* (IF: 5.235)

Book Chapters with acknowledgments at the 5D-nanoP project

1. Carlo Maria Carbonaro, Leon Engelbrecht, Chiara Olla, Antonio Cappai, Maria Francesca Casula, Claudio Melis, Luigi Stagi, Aatto Laaksonen and Francesca Mocci, Graphene Quantum Dots and Carbon Nanodots: modelling of zero-dimensional carbon nanomaterials, in *Zero dimensional carbon nanomaterials: Material design methods, properties and applications*, Editor: J. Kuruvilla, Elsevier Science (2021).

Participation at Conferences/Symposiums with acknowledgments at the 5D-nanoP project (min. 5)

1. A. Laaksonen, *Inverse Problems and Hierarchical Multiscale Modelling of Biological Matter*, Biodynamics – a Transdisciplinary Approach, Bucharest, May 19-21 organized by Romanian Academy & Institute of Biodynamics (**Invited Speaker**)
2. C. Deleanu, Some tips and tricks for NMR metabolomics and lipidomics, Magnetic Moments in Central Europe 2022 (MMCE 2022), 01-04th of June 2022, Primošten, Croatia (**Invited Speaker**)

3. D.M. Suflet, I. Popescu, I.M. Pelin, D. Serbezeanu, A.A. Enache, M. Bercea, *Polysaccharide-based electrospun nanofibers. Preparation and characterization*, Proceedings, International Conference on Rheology "Understanding the Viscoelastic Behavior of Materials – Progress and Challenges", May 26th, 2022, Iasi, Romania, pp. B15-B19 (Online scientific event) (**Proceedings**)
4. G. Fundueanu, B. Cosman, S. Bucatariu, M. Constantin, *Smart microparticulate systems for the transport and controlled delivery of doxorubicin to tumor cells*, 32nd Edition of the International Congress of Apollonia University "Preparing the future by promoting excellence", 28.02-1.03.2022, Iasi, Romania (**Oral Presentation**)
5. B. Cosman, M. Constantin, M. Bercea, G.L. Ailiesei, G. Fundueanu, *pH/thermosensitive copolymer with gelling properties for controlled delivery of drugs*, 32nd Edition of the International Congress of Apollonia University "Preparing the future by promoting excellence", 28.02-1.03.2022, Iasi, Romania (**Oral Presentation**)
6. I.M. Pelin, I. Popescu, D.L. Ichim, M. Constantin, G. Fundueanu, *Synthesis, characterization and biological activity of Pullulan-PVA hydrogels loaded with Calendula officianilis extract*, 32nd Edition of the International Congress of Apollonia University "Preparing the future by promoting excellence", 28.02-1.03.2022, Iasi, Romania (**Oral Presentation**)
7. S. Bucatariu, B. Cosman, M. Constantin, G. Fundueanu, *An interpenetrating polymeric scaffold based on hyaluronic acid and a thermosensitive polymer for biomedical applications*, 32nd Edition of the International Congress of Apollonia University "Preparing the future by promoting excellence", 28.02-1.03.2022, Iasi, Romania (**Oral Presentation**)
8. M. Zaltariov, N. Vornicu, M. Cazacu, C. Tugui, B.I. Ciubotaru, *Silicone materials-from cultural heritage conservation to biomedical applications*, International Scientific Conference "Yesterday's cultural heritage - implications for the development of tomorrow's sustainable society" 5th edition. Scientific event held in the context of the International Day of Women in Science - February 22, 2022, Chisinau – conference (**Oral Presentation**)
9. M.F. Zaltariov, A. Bargan, D. Peptanariu, C. Cojocaru, B.-I. Ciubotaru, M. Cazacu, *Bioactive and biodegradable silatranes as potential functional entities for nanoplatforms of biomedical relevance*, International Congress of the "Apollonia" University of Iasi Preparing the future by promoting excellence, XXXII Edition, February 28 - March 2, 2022, Iasi, Romania – oral communication (**Oral Presentation**)
10. A.-D. Bendrea, L. Cianga, G.-E. Hitruc, I. Popescu, I. Cianga, *Enzyme-activatable nanoplatforms based on PEG-grafted π-conjugated amphiphilic copolymers designed for synergistic cancer diagnosis and dual-mode photodynamic and chemotherapy*, Congresul International "Pregatim viitorul promovand excelenta", Editia a XXXII-a Universitatea "Apollonia" IASI, 28 februarie-2 martie 2022 (**Oral Presentation**)
11. A.-D. Bendrea, L. Cianga, E.Armelin, C. Aleman, I. Cianga, *Conjugated electroactive polymers as advanced materials for tissue engineering: The "hairy-rod" architecture as an emerging alternative*, The 3rd International Congress on Advanced Materials Science and Engineering, AMSE 2022, 21-25 July 2022, Opatija, Croatia; https://www.istci.org/AMSE2022/ (**Oral Presentation**)
12. D.M. Suflet, I. Popescu, I.M. Pelin, D. Serbezeanu, A.A. Enache, M. Bercea, *Polysaccharide-based electrospun nanofibers. Preparation and characterization*, International Conference on Rheology Understanding the Viscoelastic Behavior of Materials – Progress and Challenges, May 26th, 2022, Iasi, Romania (**Poster**)
13. M. Calin, C.A. Mocanu, G. Voicu, F. Safciuc, I. Manduteanu, M. Simionescu, *Endothelium-targeted RAGE-shRNA nanocarriers reduce atherosclerosis-associated inflammation*, 7th International Congress on Biomaterials & Biosensors (BIOMATSEN2022), 22-28 April 2022, Fethiye – Mugla, Turkey (**Poster**)
14. M. Turtoi, M. Anghelache, M. Deleanu, G. Voicu, F. Safciuc, A.A. Patrascu, D-L. Popescu, M. Calin, *Design and antitumor activity of a new vanadium-based compound*, The 19th International Conference on Nanosciences & Nanotechnologies (NN22), 5-8 July 2022, Thessaloniki, Greece (on-line) (**Poster**)

5D-nanoP Meetings between partners

January 27, 2022, 12-16 h, Petru Poni Institute, Iasi, Romania (online)
March 18, 2022, 10-16 h, Petru Poni Institute, Iasi, Romania (online)

5D-nanoP Workshop, June 15, 2022, 10-18 h, Petru Poni Institute, Iasi, Romania (online**)**

Andrei Neamtu "Unorthodox hybrid MD simulations of ion channels"
Tudor Vasiliu "On the minor groove binders"
Dragos Isac "Simulating a heterografted polythiophene copolymer. A comparison between implicit and explicit solvent models"

5D-nanoP research stay (min. 1): Natalia Simionescu at Institute of Cellular Biology and Pathology "Nicolae Simionescu" (2 weeks)

Project director,

Prof. Aatto Laaksonen